International Journal of Solids and Structures 305 (2024) 113086

Contents lists available at ScienceDirect

International Journal of Solids and Structures

journal homepage: www.elsevier.com/locate/ijsolstr

Investigating the influence of stress on UV-induced degradation in cellulose acetate: A comprehensive experimental characterization

Keven Alkhoury [a], Chi Zhang [a], Guangliang Liu [b], Kathleen McEnnis [b], Laurence Brassart [c], Siva P.V. Nadimpalli [d], Shawn A. Chester [a,*]

[a] Mechanical Engineering, New Jersey Institute of Technology, Newark, NJ 07102, USA
[b] Otto H. York Department of Chemical and Materials Engineering, New Jersey Institute of Technology, Newark, NJ 07102, USA
[c] Department of Engineering Science, University of Oxford, Oxford OX1 3PJ, United Kingdom
[d] Department of Mechanical Engineering, Michigan State University, East Lansing, MI 48824, USA

ARTICLE INFO

Keywords:
Degradable polymers
UV-induced degradation
Photo-degradation
Constitutive behavior
Stress effects

ABSTRACT

Renewable and degradable polymers have emerged in everyday applications ranging from mundane eating utensils to high-tech medical devices. However, the current literature lacks a thorough experimental characterization of the mechanical behavior change due to degradation. In this work, we characterize the microscopic chemical changes due to photo-degradation and resulting stress effects on the mechanical behavior of cellulose acetate, a renewable and degradable polymer that is used in various consumer products. Specifically, we photo-degrade this polymer under (i) traction-free conditions and (ii) under applied stress. A key finding of this work is that upon photo-degradation, this material undergoes chain scission, which affects its mechanical properties and may be further affected by the applied stress.

1. Introduction

While petrochemical-based polymers are ubiquitous in everyday life because of their many advantages such as low cost, high-speed production, and high mechanical performance, modern research is focused on replacing this class of non-sustainable polymers with renewable and degradable polymers having similar performance during their service life (Eerhart et al., 2012; Zhu et al., 2016; Elsawy et al., 2017; Nakajima et al., 2017; Asgher et al., 2020).

When in service, degradable materials are prone to damage. Damage could be caused by omnipresent environmental conditions such as moisture, temperature, UV radiation, among others (Pasparakis et al., 2012; Delplace and Nicolas, 2015). Consequently, it is important to understand the effect of degradation on the mechanical behavior of such materials to mitigate unexpected failures. While all avenues of degradation are equally important, we focus this work on photo-degradation, also often referred to as photo-oxidation. Photo-degradation is a reaction where UV irradiation, in the presence of oxygen, results in the cleavage of the polymeric backbone, breaking down the polymer chain, therefore reducing the average molecular weight (Tsuji et al., 2006).

We have chosen to use cellulose acetate in our work due to its ubiquity and numerous applications. Cellulose-derived materials, also known as cellulose esters, have gained a lot of interest for their many important applications, such as in modern coatings, optical films, and controlled release of actives, such as drugs, chemicals, etc. These actives could be used in various fields ranging from pharmaceutical, to pest control, and agriculture, among others (Edgar et al., 2001; Barud et al., 2008; Fischer et al., 2008; Galiano et al., 2018). In addition to their wide range of applications, cellulose esters are both renewable and degradable, making them environmentally friendly materials of interest (Edgar et al., 2001).

The mechanisms of photo-degradation for cellulose acetate are widely discussed in literature (Al-Abri et al., 2019; Yadav and Hakkarainen, 2021; Parida et al., 2022), and the main reaction can be described as follows. Upon photo-degradation, the cellulose acetate backbone undergoes chain scission, as shown in Fig. 1, which reduces the overall molecular weight of the original material, and results in a smaller polymer.

There is abundant literature available on the topic of photo-degradation in the chemical engineering community. For instance, one may find a wide range of highly cited articles on the topic of photo-degradation in high-impact journals, relatively unknown to mechanicians but widely read by chemical engineers (Celina, 2013; La Mantia et al., 2017, and references within). Relevant to this work, Shyichuk et al. (2001) investigated the effect of tensile stress on chain-scission and cross-linking during photo-oxidation of polypropylene, while White and Shyichuk (2007) derived chain-scission and cross-linking rates

* Corresponding author.
E-mail address: shawn.a.chester@njit.edu (S.A. Chester).

https://doi.org/10.1016/j.ijsolstr.2024.113086
Received 24 July 2024; Received in revised form 1 September 2024; Accepted 24 September 2024
Available online 3 October 2024
0020-7683/© 2024 Elsevier Ltd. All rights are reserved, including those for text and data mining, AI training, and similar technologies.

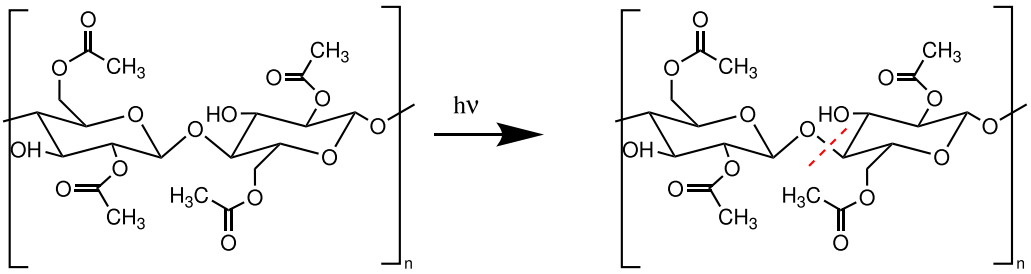

Fig. 1. Possible chain scission reaction (indicated by the dashed line) driving the photo-degradation in cellulose acetate.

of multiple polymers using gel permeation chromatography (GPC), among others. Furthermore, there exists a substantial amount of historical work dedicated to the characterization of the effect of photo-degradation on the mechanical properties of polymers (Mai et al., 1980; Hamid, 2000; Van de Velde and Kiekens, 2002; Tsuji et al., 2006, and references within). In studies conducted over the last decade, Belbachir et al. (2010) investigated the effect of accelerated UV aging on polylactic acid (PLA) on both the mechanical response and chemical structure of the degraded polymers. Rodriguez et al. (2020) studied the effect of UV-aging on the mechanical fracture behavior of low-density polyethylene (LDPE). Additionally, Najmeddine et al. (2022) investigated the effect of photo-degradation on the physio-chemical changes of LDPE.

In the previously mentioned studies that investigated changes in mechanical properties, photo-degradation experiments were limited to traction-free conditions. While some of these studies investigated the effect of photo-degradation on the underlying chemistry of the polymers of interest, to the best of the authors' knowledge, there exists no comprehensive work that addresses both stress effects and the underlying chemistry simultaneously. The work of Briassoulis (2005) stands as the singular attempt in this context, where they investigated the effect of tensile stress on the mechanical behavior of photo-degrading LDPE only, without addressing the underlying chemistry.

The objective of this work is to characterize microscopic chemical changes due to photo-degradation and the resulting stress effects on the mechanical behavior of cellulose acetate. Towards the objective, we have conducted a comprehensive experimental program that consists of first degrading cellulose acetate under (i) traction-free conditions, and (ii) under applied stress, and then testing the effect of degradation on the materials' response. The tests that we perform can be split into two groups: those that aim to uncover micro-scale chemical/molecular information and those that aim to uncover macro-scale mechanical behavior. The tests aimed at obtaining molecular information consist of gel permeation chromatography (GPC), thermogravimetric analysis (TGA), differential scanning calorimetry (DSC), and Fourier-transform infrared spectroscopy (FTIR). These help in understanding the micro-scale effect of stress-enhanced photo-degradation on the chemical structure of the material. The macro-scale experiments consist of uniaxial tension tests to characterize the effect of stress-enhanced photo-degradation on the macro-scale constitutive response of the material.

The remainder of this paper is organized as follows. In Section 2, we provide the background information required alongside the major assumptions that underpin our experimental program. In Section 3, we provide a summary of the photo-degradation apparatus and procedure. In Sections 4 and 5, we present the experiments performed to obtain micro-scale and macro-scale data, respectively. In Section 6, we summarize the results and propose a potential mechanism. In Section 7, we provide concluding remarks for this work.

2. Background and assumptions

In this Section, we provide the non-traditional background information required alongside two major assumptions that underpin our experimental methods in characterizing the stress effects during photo-degradation on the mechanical behavior of cellulose acetate.

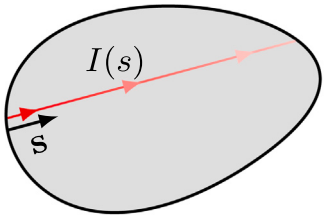

Fig. 2. Schematic of a monochromatic light attenuation as it travels through a participating medium in a given direction denoted by the unit vector **s**.

Table 1
Beer–Lambert model parameters obtained from the fit in Fig. 3.

I_0 (mW/cm^2)	β (μm^{-1})
2.59	0.007

2.1. Attenuation of light

As monochromatic light travels through a participating medium in a given direction, it is well known that its amplitude attenuates, a phenomenon based on physical observation, often called the Beer–Lambert Law (Lambert, 1760), which can be schematically described by Fig. 2.

This phenomenon is commonly modeled using

$$I(s) = I_0 \exp(-\beta s), \tag{1}$$

where I_0 is the incident intensity, β the attenuation coefficient, and s is the path length. This attenuation is relevant for photo-degradation since the attenuation results in an inhomogeneous intensity distribution across the sample thickness during exposure. That results in an inhomogeneous degradation across our sample, which must be mitigated as much as possible for a clear interpretation of the experimental results.

Towards mitigating inhomogeneity, we first measure the incident light intensity using a UV light meter (Omega-HHUV254SD), as well as measuring the light intensity across cellulose acetate samples of relevant thicknesses, as shown in Fig. 3. We observe that the light was completely attenuated for a sample size of 254 μm, which is approximately twice the size of our samples. We then fit the measurements using (1), and Fig. 3 shows a reasonable agreement between the "Beer–Lambert" model fit and experimental results. Moreover, the parameters are tabulated in Table 1.

To the best of the authors' knowledge, most of the existing literature tries to mitigate attenuation by reducing the thickness of the sample (Tsuji et al., 2006; Belbachir et al., 2010; Ayoub et al., 2020; Najmeddine et al., 2022). However, as we observe from Fig. 3, attenuation could be significant even for very thin samples and, therefore, cannot be always neglected. For that reason, and towards mitigating the inhomogeneous degradation across our samples, we use two UV sources, one from each side, as shown schematically in Fig. 4, such that our sample is exposed from both sides. Since light emanating from two independent sources (such as UV lamps in our experiments) of

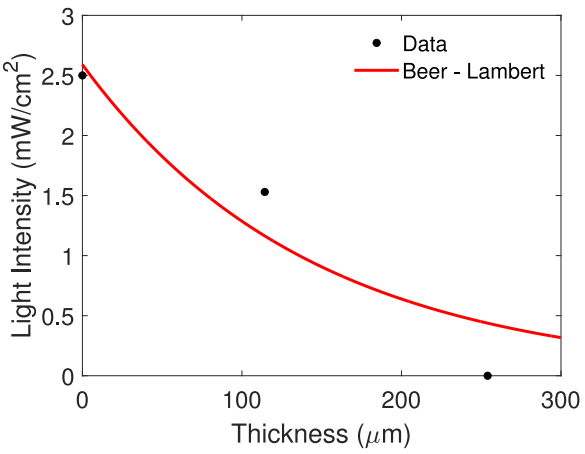

Fig. 3. Light attenuation measurements along with the corresponding Beer–Lambert model for cellulose acetate samples of varying thicknesses.

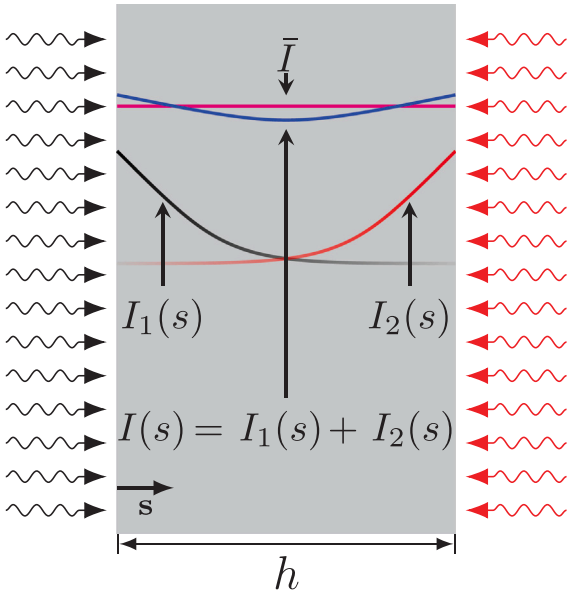

Fig. 4. Schematic of light attenuation across the sample thickness and the approximated quasi-uniform "average intensity" $\bar{I}$.

intensities I_1 and I_2 is incoherent, when combined, leads to $I(s) = I_1(s) + I_2(s)$ (Hecht, 2002), which we approximate by an "average intensity"

$$\bar{I} = \frac{1}{h}\int_0^h I(s)\,ds\,, \tag{2}$$

where the "average intensity" $\bar{I}$ is assumed to be quasi-uniform, resulting in a *nearly* homogeneous degradation across the thickness, as shown schematically in Fig. 4. This is the first major assumption we make for analysis of the experimental results.

In the case that β is a constant and does not vary in space, this leads to the simple result

$$\bar{I} = \frac{1}{h}\int_0^h I_0\exp(-\beta s) + I_0\exp\big(-\beta(h-s)\big)ds\,, \tag{3}$$

which in this case leads to an average intensity $\bar{I}$

$$\bar{I} = \frac{2I_0}{\beta h}\left[1-\exp\left(-\beta h\right)\right]\,. \tag{4}$$

2.2. Degradation mechanisms

All degradation experiments were conducted at a constant temperature of 27 °C. In addition to that, since all of our degradation experiments occurred over a short period of time, we neglect any possible degradation due to physical aging, as well as thermal oxidation, since both are expected to happen at a relatively longer time scale and much higher temperatures (Yousif and Haddad, 2013; Gardette et al., 2013; Rasselet et al., 2014). Furthermore, we characterized the mass change in our photo-degraded samples using a balance (Sartorius Practum213-1S), and were unable to measure any mass change with an accuracy of 0.3%, where the sample was 313 mg and the balance has an accuracy of 1 mg. Therefore our second major assumption is that we attribute any measurable change in either the micro-scale or macro-scale behavior of cellulose acetate in this work to photo-degradation alone.

2.3. Baseline and degraded materials

When discussing materials undergoing degradation, two terms describing the state of the material are necessary to understand — virgin and degraded. Virgin material is a raw material without any prior degradation and loading history, serving the purpose of establishing a baseline behavior for comparison. Whereas degraded material is a material that has been subjected to degradation under different conditions (UV dose and stress), and is used to understand the effect of these conditions on the materials' response.

3. Photo-degradation apparatus and procedure

Prior to photo-degradation, commercially purchased cellulose acetate film is subjected to a stress relief heat treatment for 6 h at a temperature of 135 °C, followed by a slow cooling to room temperature overnight.[1] Then, tensile dog bone samples are extracted using an ASTM D638-V cutting die. The nominal gauge section dimensions of our samples are ≈9.52 mm long, ≈3.14 mm wide, and ≈0.114 mm thick, though the exact dimensions of each sample are measured prior to testing for accuracy. The grip sections are then covered by tape, as can be seen in Fig. 5, to prevent any exposure to UV light and thus eliminate any possible degradation to these regions. Next, samples are gripped and exposed to UV light at a known intensity for a fixed amount of time, commonly referred to as "UV dose" expressed in mJ/mm^2. We photo-degrade cellulose acetate samples using two 20 W UV lamps (Analytik Jena XX-20S) with a wavelength $\lambda = 254$ nm, that corresponds to UVC on the UV spectrum. Specifically, the 20 W lamps are set at a standoff distance of 0.3 m, which leads to an incident intensity of $I_0 = 2.5$ mW/cm^2. In what follows, the average intensity $\bar{I}$ is used to compute the UV dose. Moreover, the chosen exposure times for this work are four (4), eight (8), and twelve (12) hours, resulting in UV doses of 494 mJ/mm^2, 988 mJ/mm^2, and 1482 mJ/mm^2, respectively.

Our degradation experiments can be grouped into two categories: (i) traction-free degradation and (ii) degradation under a constant applied stress. For the traction-free degradation experiments, the samples are gripped from one end, hung under their own weight, and exposed to UV light, as shown in Fig. 5a. Those experiments provide a baseline behavior of photo-degrading cellulose acetate. For the degradation under constant applied stress, the samples are gripped from one end, and known constant stress is applied from the other end, resulting in a constant tensile state of stress, as shown in Fig. 5b. Those experiments allow us to probe the effect of stress on the mechanical behavior of photo-degrading cellulose acetate. The results from those experiments are reported in terms of engineering stress; (i) due to

[1] The cooling is uncontrolled in practice; the power was turned off, and the oven door was not opened until the next day.

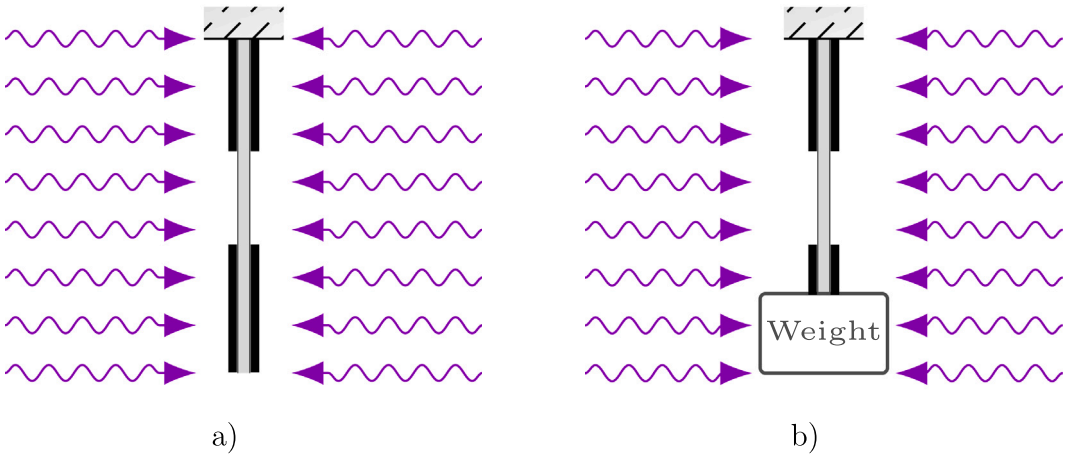

Fig. 5. A schematic cross-section of the experimental setup used for (a) traction-free degradation, and (b) degradation under constant applied stress. Note that the UV light comes from both sides and that the grip section is taped, represented by the black in the figure, leaving only the gauge section open to UV light.

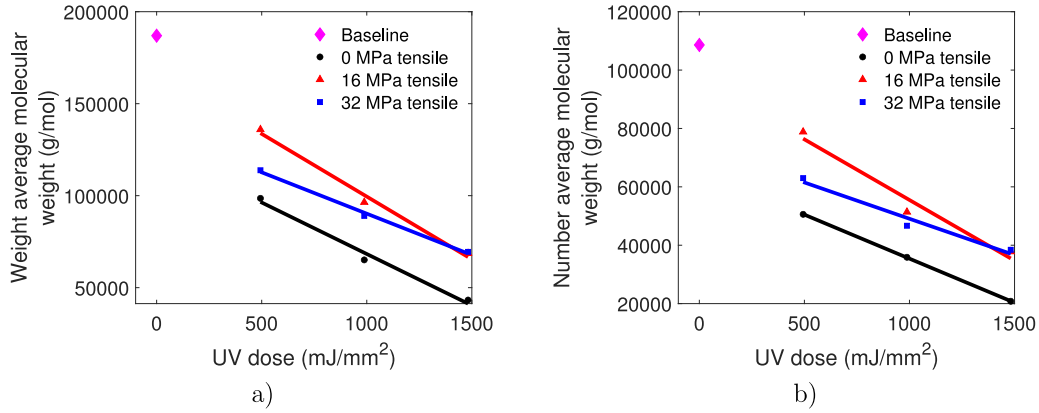

Fig. 6. Typical GPC results showing the (a) weight average molecular weight (M_w), (b) number average molecular weight (M_n), for cellulose acetate subjected to different UV doses and applied stress. Note that the GPC curves for all the loading scenarios are reported in Appendix A for completeness (see Figs. 17, 18, 19, and 20).

its simplicity, ubiquity, and acceptance by many other communities, and (ii) since our current setup does not allow us to measure any potential creep[2] while photo-degrading materials under the prescribed stress. We also note that any stress contribution due to the samples' weight was neglected in the traction-free degradation experiments as the samples typically weighed ≈0.025% of the smallest applied load (1.34 lbs), and therefore is neglected. Moreover, five samples are used in each degradation experiment, and each degradation experiment is repeated at least once to ensure repeatability between the results. Lastly, photo-degraded samples are used to characterize the micro-scale and macro-scale response.

4. Experiments to obtain the micro-scale response

We perform chemical analysis and characterization tests to understand the effect of stress-enhanced photo-degradation on the micro-scale response or the chemical structure of the material. We note that the samples used in those tests were extracted from the degraded samples' gauge section, with the exception of a virgin sample extracted from raw material without any prior degradation and loading history, as it provides us with a baseline behavior for comparison. GPC is used to investigate changes in the molecular weight. TGA is used to investigate the thermal stability. DSC is used to investigate the change in the glass transition temperature, T_g, and FTIR is used to investigate the change in the functional group structural information. We discuss the details of each experiment in what follows.

4.1. Gel permeation chromatography (GPC)

4.1.1. Procedure

Gel permeation chromatography (GPC) analyses were performed by analyzing samples in dimethyl formamide (0.5 mL/min) using a *Waters Breeze* system that was equipped with a 1525 binary HPLC pump, a 717plus autosampler, and a 2414 refractive index detector. For separation, the samples were passed through a series of styragel columns (*Polymer Laboratories*, PLgel 5 μm guard, one PLgel 10 μm MIXED-B and one PLgel 5 μm MIXED-C column), which were kept in a column heater at 50 °C. The columns were calibrated with narrow polymethyl methacrylate standards (12) in the molecular weight range of 800 to 2,200,000 Da. Instrument operation and data analysis were performed using *Empower* software.

4.1.2. Results

Typical GPC results reporting on the weight average molecular weight (M_w), and the number average molecular weight (M_n) are shown in Fig. 6. For completeness, all the GPC curves are provided in Appendix A. It is evident from Fig. 6a and b that an increase in the UV dose leads to a decrease in both the weight average molecular weight (M_w), and the number average molecular weight (M_n), regardless

[2] We note that in the absence of UV light there was no measurable creep in our samples under an applied stress of 32 MPa tensile for more than 12 h.

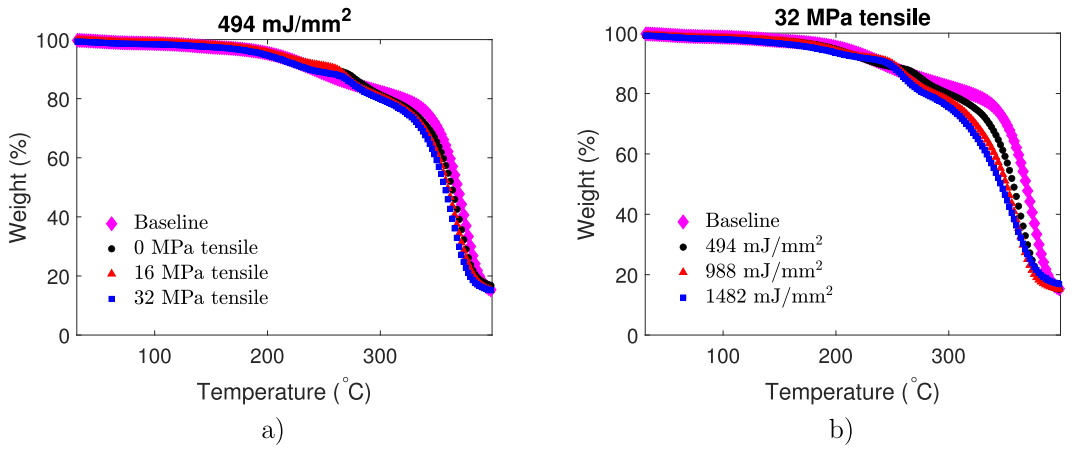

Fig. 7. Typical TGA weight (%) — temperature (°C) results for cellulose acetate (a) comparing the effect of the applied stress under a UV dose of 494 mJ/mm^2, and (b) comparing the effect of the UV dosage under an applied tensile stress of 32 MPa. Note that the results for all the loading scenarios are reported in Appendix B for completeness (see Fig. 21).

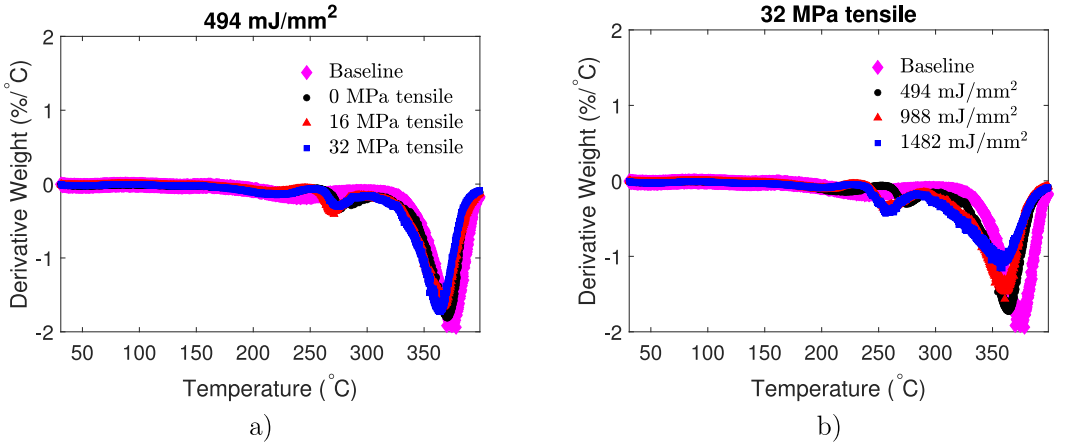

Fig. 8. Typical TGA derivative weight (%/°C) — temperature (°C) results for cellulose acetate (a) comparing the effect of the applied stress under a UV dose of 494 mJ/mm^2, and (b) comparing the effect of the UV dosage under an applied tensile stress of 32 MPa. Note that the results for all the loading scenarios are reported in Appendix B for completeness (see Fig. 22).

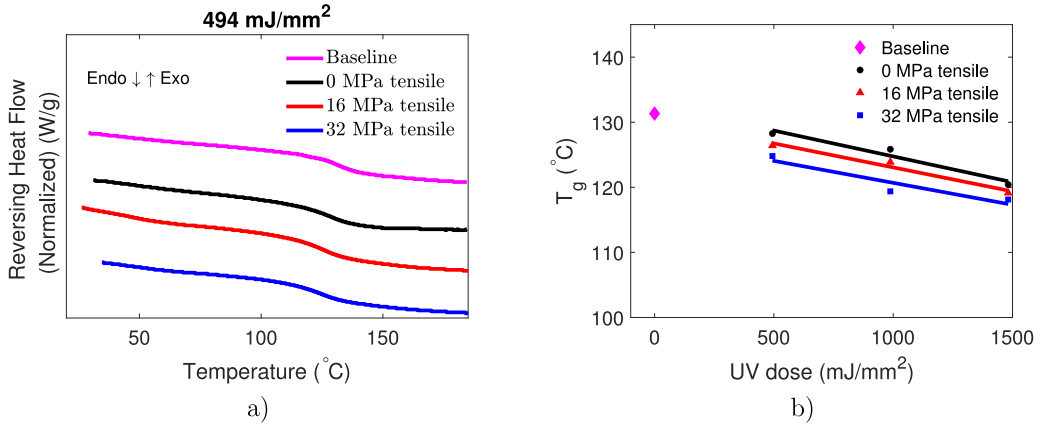

Fig. 9. (a) Typical DSC results for cellulose acetate subjected to different UV doses and applied stress and (b) the corresponding T_g results. Note that the results for all the loading scenarios are reported in Appendix C for completeness (see Fig. 23).

of the applied stress. Further analysis of the rate of change in M_w and M_n was conducted by fitting a line to the data for each applied stress scenario for different UV doses, and the corresponding slope is tabulated in Table 2. The results suggest that although the specific applied stress might affect both the M_w and M_n, the overall trend of the rate of change remains unchanged: as the UV dose increases, M_w and M_n decrease. And since GPC results are typically relative, we refrain from concluding about stress effects based on these results alone, and we save such analysis for after the macro-scale tests, where we have done a comprehensive analysis to check for statistical significance.

Moreover, the polydispersity Index (PDI), defined as M_w/M_n is tabulated in Table 3, and it can be observed that regardless of the

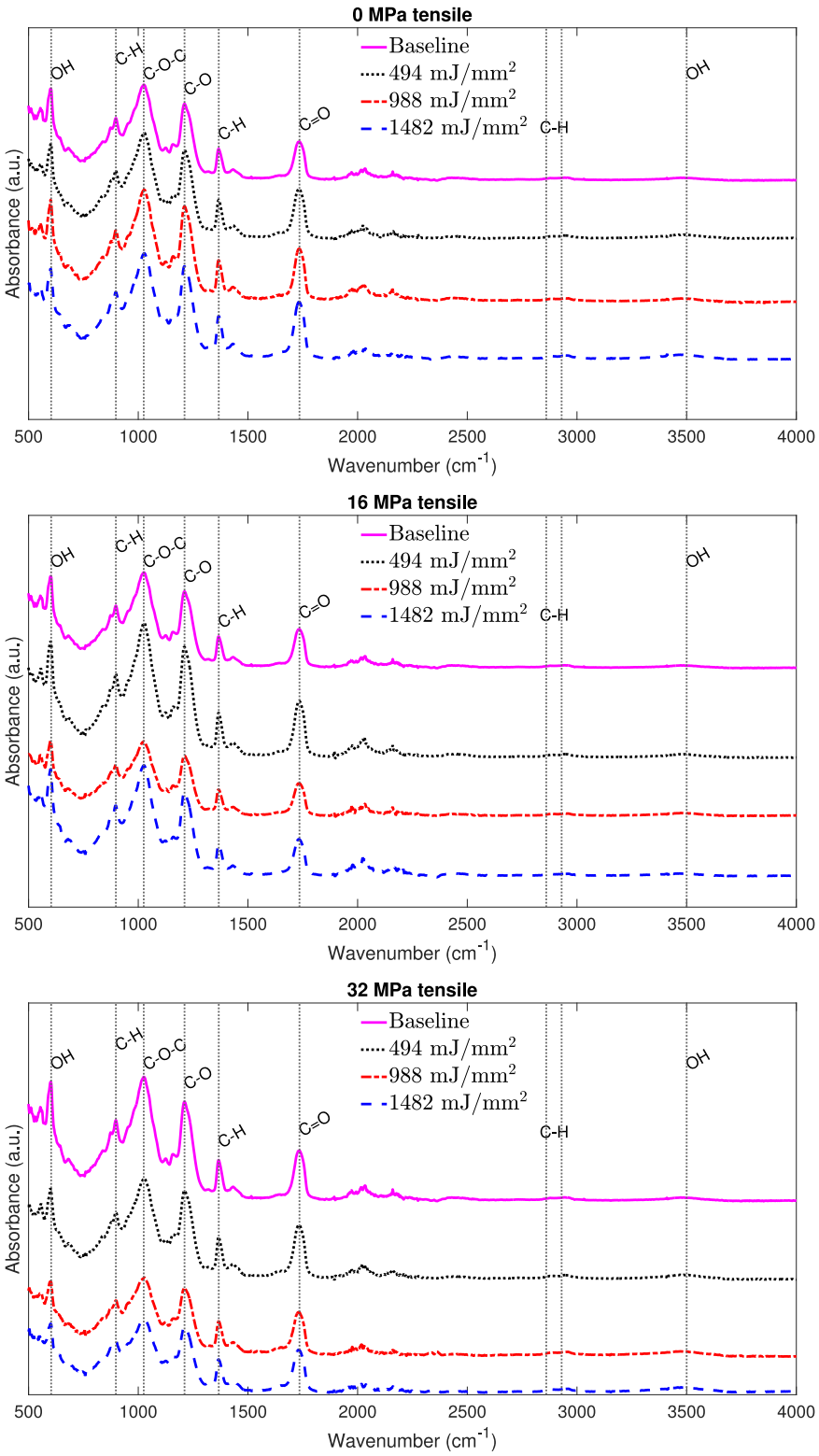

Fig. 10. ATR-FTIR spectrum for cellulose acetate subjected to different UV doses and applied stress.

applied UV dose or applied stress, the PDI value is higher than the baseline value.

4.2. Thermogravimetric analysis (TGA)

4.2.1. Procedure

Thermogravimetric analyses were performed using a Perkin Elmer 8000 TGA to check for any possible change in the decomposition reactions due to UV exposure and to ensure that other experiments were performed prior to the release of volatiles. Both virgin and photo-degraded samples were tested following a heating cycle from 30 °C – 400 °C at a rate of 10 °C/min, under a nitrogen atmosphere.

4.2.2. Results

Typical TGA results reporting on the weight loss and the first derivative of the weight loss of cellulose acetate, as a function of temperature,

Table 2
Measured slope ($\frac{g/mol}{mJ/mm^2}$) from GPC results for cellulose acetate subjected to different UV doses and applied stress.

Applied stress	0 MPa tensile	16 MPa tensile	32 MPa tensile
M_w slope ($\frac{g/mol}{mJ/mm^2}$)	−55.96	−68.15	−44.92
M_n slope ($\frac{g/mol}{mJ/mm^2}$)	−30.14	−41.53	−24.86

Table 3
PDI results, defined as M_w/M_n for cellulose acetate subjected to different UV doses and applied stress.

UV dose (mJ/mm^2) \ Applied stress	0 MPa tensile	16 MPa tensile	32 MPa tensile
0 (baseline)	1.72	N/A	N/A
494	1.95	1.81	2.08
988	1.73	1.88	1.82
1482	1.81	1.91	1.81

Table 4
Measured slope ($\frac{°C}{mJ/mm^2}$) from DSC results for cellulose acetate subjected to different UV doses and applied stress.

Applied stress	0 MPa tensile	16 MPa tensile	32 MPa tensile
Slope ($\frac{°C}{mJ/mm^2}$)	−0.0079	−0.0074	−0.0068

are shown in Figs. 7 and 8, respectively. It can be observed from Figs. 7a and 8a that for a constant UV dose of 494 mJ/mm^2, degradation under stress does not affect the thermal decomposition of cellulose acetate, while Fig. 7b and 8b show that for constant applied tensile stress of 32 MPa, the thermal decomposition changes with different UV doses. Specifically, as the UV dose increases, the curves shift to the left, indicating that cellulose acetate becomes more susceptible to thermal decomposition, regardless of the applied stress. We note that the same trend for all results holds for all the loading scenarios and are reported in Appendix B for completeness. These results suggest that only the UV dose has an effect on the thermal decomposition temperature of photo-degrading cellulose acetate.

4.3. Differential scanning calorimetry (DSC)

4.3.1. Procedure

Modulated DSC analyses were conducted using a TA Instruments DSC 250 along with the Refrigerated Cooling System 40 (RCS 40). Samples weighing 3 to 5 mg were sealed in Tzero pans with Tzero lids. A reference pan was also sealed. Heating occurred at a rate of 5 °C/min from 20 °C to 180 °C, with a 5 °C modulation for 60 s. Measurements were carried out under pure nitrogen. T_g was determined by analyzing the inflection point in the reversing heat flow curves, where a typical curve is reported in Fig. 9a. It is noted that the results for all loading scenarios are provided in Appendix C.

4.3.2. Results

It is evident from the T_g values shown in Fig. 9b that an increase in the UV dose leads to a decrease in the T_g regardless of the applied stress. Further analysis of the rate of change in T_g was conducted by fitting a line to the T_g data for each applied stress scenario for different UV doses, and the corresponding slope is tabulated in Table 4. The results suggest that although the specific applied stress might affect the T_g, the overall trend of the rate of change remains unchanged, as the UV dose increases the overall T_g decreases. We also note that while the data presented in Fig. 9b may suggest that the applied stress plays a role in decreasing T_g, we save such analysis for after the macro-scale tests, where we have done a comprehensive analysis to check for statistical significance.

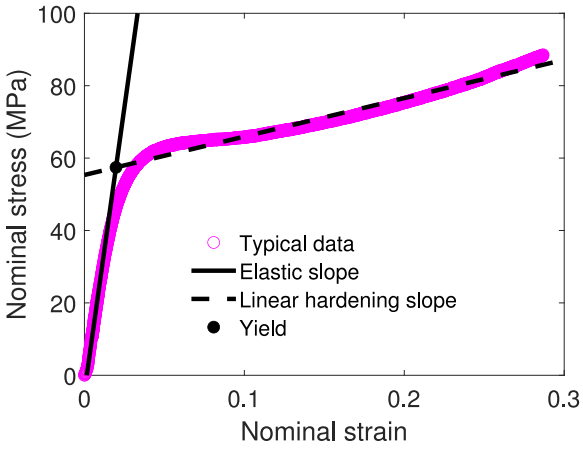

Fig. 11. Schematic showing the method to determine the yield strength using the intersection of elastic and linear hardening slopes for a typical uniaxial experimental result.

4.4. Fourier-transform infrared spectroscopy (FTIR)

4.4.1. Procedure

Attenuated total reflectance (ATR) FTIR measurements were conducted using an Agilent Cary 670 Spectrometer coupled with a micro-diamond ATR, to analyze the functional group structural information. Virgin and degraded cellulose acetate films were tested under a wide spectrum range (500 cm^{-1}– 4000 cm^{-1}). We note that all the samples used in this study were tested to check for repeatability, but only one data set for each condition is shown here for clarity.

4.4.2. Results

The FTIR results are shown in Fig. 10, displaying peaks at 603 cm^{-1}, 898 cm^{-1}, 1025 cm^{-1}, 1211 cm^{-1}, 1367 cm^{-1}, and 1735 cm^{-1} that corresponds to OH out of plane deformation, C–H out of plane deformation, C–O–C asymmetric stretching, C–O asymmetric stretching, C–H symmetric bending, C=O bond of the ester group in the polymer, respectively. At higher wavenumbers, three weak broad bands are observed, where 2860 cm^{-1} and 2930 cm^{-1} correspond to C–H asymmetric, and at 3465 cm^{-1} can be attributed to OH groups in external absorbed water molecules, similarly to what was reported in literature (Santos-Sauceda et al., 2021). It can also be seen from Fig. 10 that the results exhibit similarity across different UV doses and applied stress, which suggests that while there might be a subtle change, the UV degradation, both under stress and traction-free, did not significantly alter the functional groups in cellulose acetate. This suggests that degradation is predominantly through a mechanism that does not alter the functional groups, such as chain scission.

4.5. Discussion & summary of the experiments to obtain the micro-scale response

We observed from the GPC results that an increase in the UV dose leads to a decrease in both M_w and M_n, regardless of the applied stress. Furthermore, we observed from TGA results that for a constant UV dose, degradation under stress does not affect the thermal decomposition of cellulose acetate, however, for a constant applied stress, the thermal decomposition changes with different UV doses. Specifically, as the UV dose increases, the curves shift to the left, indicating that cellulose acetate becomes more susceptible to thermal decomposition, regardless of the applied stress. Additionally, we observed from the DSC results that an increase in the UV dose leads to a decrease in the T_g regardless of the applied stress, showing agreement with the molecular weight results (Fox and Flory, 1950). Moreover,

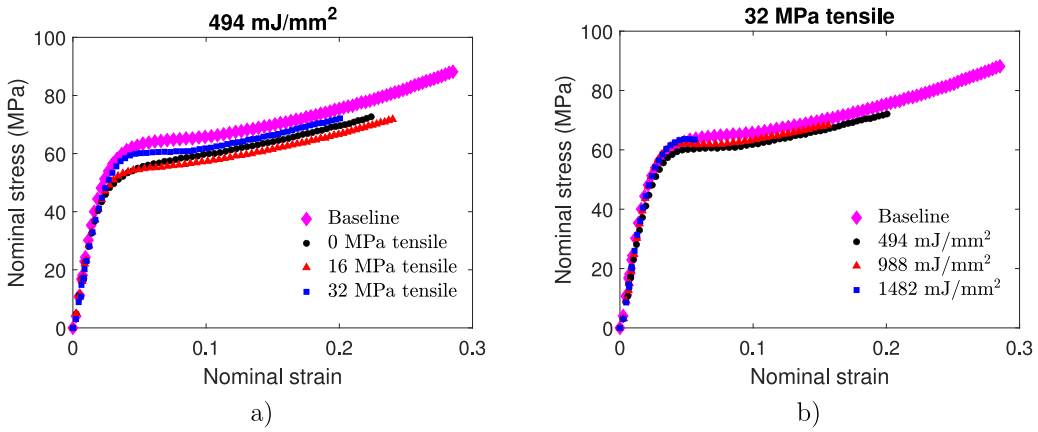

Fig. 12. Typical uniaxial experimental results for load–unload tensile tests for cellulose acetate (a) comparing the effect of the applied stress under a UV dose of 494 mJ/mm^2, and (b) comparing the effect of the UV dose under an applied tensile stress of 32 MPa. Note that the results for all the loading scenarios are reported in Appendix D for completeness (see Fig. 24).

we observed from the FTIR that the UV degradation, both under stress and traction-free, did not significantly alter the functional groups in cellulose acetate. These results suggest that upon photo-degradation, the cellulose acetate backbone undergoes chain scission, which reduces the overall molecular weight of the original material, and results in a smaller polymer with higher mobility, and thus, having a smaller T_g. And as noted previously, while both GPC and DSC results imply that the applied stress might affect both molecular weight and glass transition temperature, we save such analysis for after the macro-scale experiments, where we have performed a comprehensive analysis to check for statistical significance.

5. Experiments to obtain the macro-scale response

We perform typical uniaxial mechanical tests to understand the effect of the stress-enhanced photo-degradation on the macro-scale constitutive response of cellulose acetate. Specifically, uniaxial tensile experiments are used to calculate relevant properties such as nominal stress at break, nominal strain at break, Young's modulus, yield strength, and hardening slope for different applied stress and UV dosages. Similarly, we also test a virgin sample extracted from raw material without any prior degradation and loading history, as it provides us with a *baseline* behavior for comparison.

5.1. Preliminaries

We define the standard nominal kinematic quantities for a uniaxial test, where the nominal strain is defined by

$$\varepsilon = \frac{l - l_0}{l_0} = \frac{u + l_0 - l_0}{l_0} = \frac{u}{l_0}, \tag{5}$$

and the corresponding nominal strain rate by

$$\dot{\varepsilon} = \frac{\dot{u}}{l_0}, \tag{6}$$

where l is the instantaneous gauge length, l_0 is the initial gauge length, u is the crosshead displacement, and $\dot{u}$ is the crosshead velocity. We choose to perform our experiments under displacement control and at a constant nominal strain rate, and make use of (6) to determine the crosshead speed.

Additionally, the nominal stress P, can be obtained by dividing the force over the initial cross-sectional area A_0

$$P = \frac{F}{A_0}. \tag{7}$$

5.2. Mechanical testing

5.2.1. Procedure

We conducted uniaxial tension test at a nominal strain rate of $\dot{\varepsilon} = 10^{-3}$ s^{-1} using an MTS Criterion Model 43 uniaxial testing machine at room temperature (24 °C).[3] Prior to mechanical testing, immediately after photo-degradation, a speckle pattern is created using spray paint, as DIC requires appropriate contrast in the image. We use a 500N load cell (MTS Model LPB.502 D) to measure the force. Additionally, we make use of the non-contact Digital Image Correlation (DIC) software Vic2D (Correlated Solutions) that is integrated with a digital camera (FLIR Grasshopper3) to measure the deformation in our uniaxial tensile experiments. Our DIC data acquisition system captures images simultaneously while taking force signal measurements, making the deformation and force synchronized in time and thus minimizing post-processing efforts. All the tension tests consisted of loading and unloading the materials within their elastic limit to obtain the Young's modulus, followed by reloading until failure. The yield strength was obtained using an intersection between the elastic slope and the linear hardening slope, as schematically shown in Fig. 11.

5.2.2. Results

Typical uniaxial tension test results are shown in Fig. 12. For completeness, all the uniaxial tension test results are provided in Appendix D.

It can be observed from Fig. 12a that for a constant UV dose of 494 mJ/mm^2, degradation under various stresses has an effect on the overall stress–strain response of photo-degrading cellulose acetate. Similarly, it can be observed from Fig. 12b that for constant applied stress of 32 MPa, the overall stress–strain response under various UV doses is also affected. We note that changes are observed for all the loading scenarios but are not shown here in Fig. 12 for clarity. For that reason, we make use of the results provided in Fig. 24 (Appendix D), which shows a clear effect of both UV dose and applied stress on the overall constitutive response of our material. This allows the extraction of relevant mechanical properties, such as nominal stress at break, nominal strain at break, Young's modulus, hardening slope, and yield strength. The average value of each mechanical property is reported in Fig. 13.

Specifically, Fig. 13a shows the nominal stress at break, and it can be observed that as the UV dose increases, the material fails at

[3] While our material showed some sign of rate-dependency, we leave an inclusion of such effects to future work.

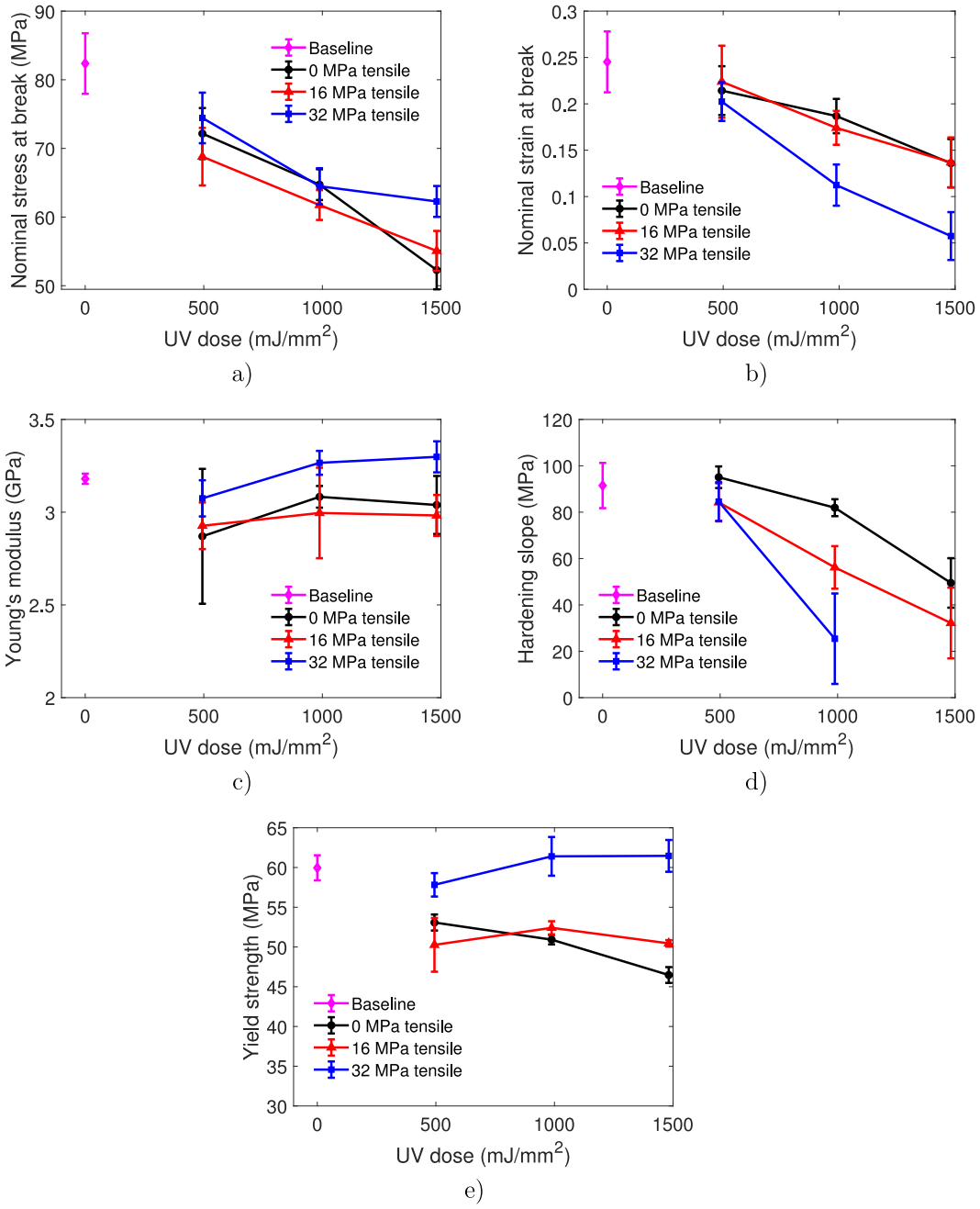

Fig. 13. Mechanical properties calculated as an average from the uniaxial experimental results (cf., Fig. 24 in Appendix D). (a) Nominal stress at break, (b) nominal strain at break, (c) Young's modulus, (d) hardening slope, and (e) yield strength, for different applied stress and UV dose. Error bars indicate the standard deviation. Note that for a UV dose of 1482 mJ/mm^2 and an applied stress of 32 MPa, the material was brittle, and did not show any hardening.

a lower stress, regardless of the applied stress. Fig. 13b shows the nominal strain at break, and it can be noted that as the UV dose increases, the strain to failure decreases, regardless of the applied stress. Fig. 13c shows Young's modulus, obtained by fitting a line to the elastic unload data, where some changes due to both UV doses and applied stress can be observed. Fig. 13d reports on the hardening slope, and it can be observed that as the UV dose increases, the hardening slope decreases, regardless of the applied stress. We note that for a UV dose of 1482 mJ/mm^2 and an applied stress of 32 MPa, the material was brittle, and did not show any hardening. Lastly, in Fig. 13e, nontrivial changes in yield strength can be observed due to both UV doses and applied stress.

5.3. Discussion & summary of the experiments to obtain the macro-scale response

While Fig. 13 shows some evidence that the UV dose affects the mechanical properties, it remains crucial to investigate if there is statistical significance due to the applied stress. Therefore, we conducted a Wilcoxon rank sum test using the MATLAB built-in function `ranksum` on each mechanical property. The comparison was made for each stress scenario, 16 MPa tensile and 32 MPa tensile, against the traction-free baseline for a fixed dose. This test aimed to check for any statistical significance, indicated by a p-value < 0.05, and represented by an $(*)$ in the boxplots. The results can be seen in Figs. 14, 15, and 16.

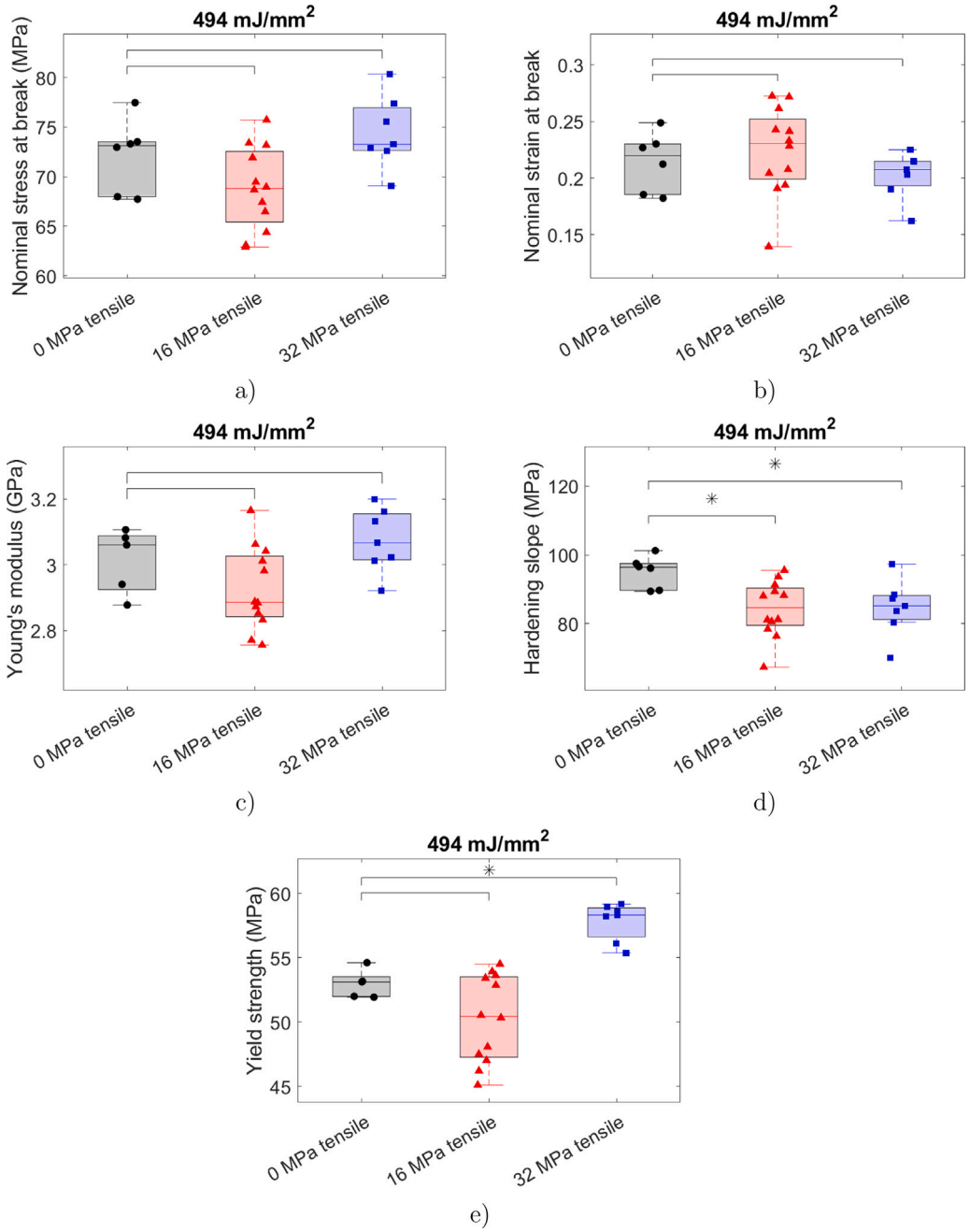

Fig. 14. Boxplots comparing the effect of applied stress on the (a) nominal stress at break, (b) nominal strain at break, (c) Young's modulus, (d) hardening slope, and (e) yield strength for a UV dose of 494 mJ/mm^2. Note that an (∗) in the plots indicates statistical significance as a result of the Wilcoxon rank sum test (p-value < 0.05).

Fig. 14 shows boxplots comparing the mechanical properties under different applied stress for a UV dose of 494 mJ/mm^2, where it can be observed that degradation under stress has no significant effects on most of the mechanical properties. Fig. 15 shows boxplots comparing the mechanical properties under different applied stress for a UV dose of 988 mJ/mm^2, where it can be observed that degradation under stress has a significant effect on some of the mechanical properties. Specifically, for a UV dose of 988 mJ/mm^2, degradation under an applied stress of 16 MPa tensile affects the nominal stress at break, the hardening slope, and the yield strength, while degradation under 32 MPa tensile affects the nominal strain at break, Young's modulus, the hardening slope, and the yield strength. Similarly, Fig. 16 shows boxplots comparing the mechanical properties under different applied stress for a UV dose of 1482 mJ/mm^2, where it can be observed that degradation under stress has a significant effect on some of the mechanical properties. Specifically, for a UV dose of 1482 mJ/mm^2, degradation under 16 MPa tensile affects the yield strength, while degradation under 32 MPa tensile affects the nominal stress at break, nominal strain at break, Young's modulus, and yield strength.

Based on the results described in Figs. 14, 15, and 16, it can be observed that the mechanical properties of photo-degrading cellulose acetate only show a statistically significant effect after a certain UV dose is reached.

6. Summary & potential mechanism

Based on the results of the micro-scale response, described in detail in Section 4.5, and summarized here for brevity, it was observed that an increase in the UV dose decreases M_w, M_n, and T_g, without having any significant effect on the functional groups in cellulose acetate regardless

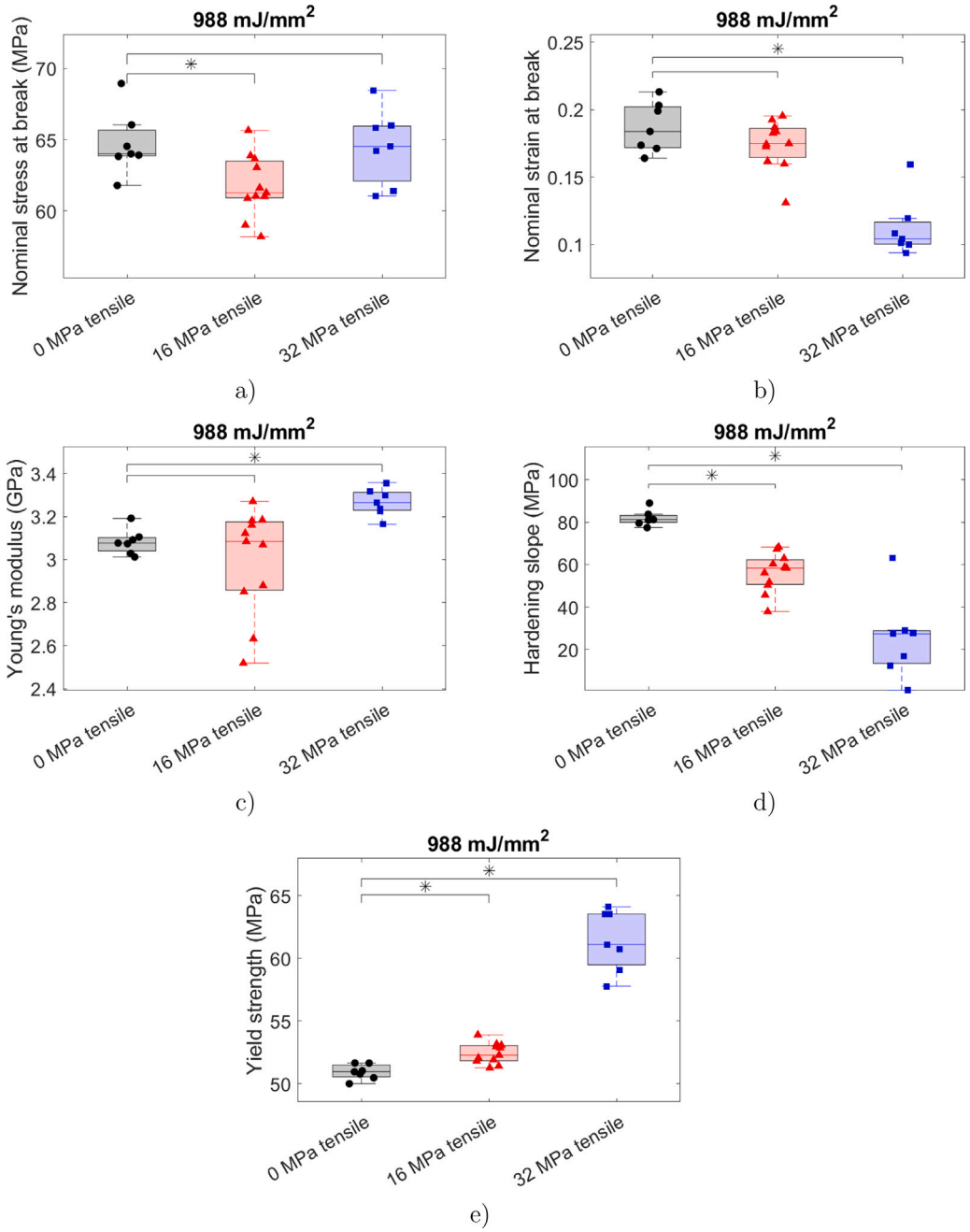

Fig. 15. Boxplots comparing the effect of applied stress on the (a) nominal stress at break, (b) nominal strain at break, (c) Young's modulus, (d) hardening slope, and (e) yield strength for a UV dose of 988 mJ/mm^2. Note that an (∗) in the plots indicates statistical significance as a result of the Wilcoxon rank sum test (p-value < 0.05).

of the applied stress. Moreover, based on the results of the macro-scale response, summarized in 5.3, it was observed that both the UV dose and applied stress affect the mechanical properties. These results suggest that upon photo-degradation, cellulose acetate undergoes chain scission, similar to what was observed in other work (Tsuji et al., 2006; Ayoub et al., 2020). Furthermore, the effect of the applied stress on the mechanical properties suggests a concurrent mechanism, which we postulate is related to the free volume. The free volume may be increased due to scission (Consolati et al., 2023), which is known to decrease the yield strength (Argon and Demkowicz, 2008).

Starting with the Young's modulus reported in Fig. 13c, we note that while some changes may be observed, the overall trend seems unaffected by both UV dose and applied stress.

Moving onto Fig. 13d, we observe a decrease in the hardening slope with increasing UV dose due to chain scission. Furthermore, this response decrease becomes more pronounced for higher applied stresses. The observed behavior suggests that during UV exposure, the application of stresses results in a "less-entangled" microstructure and, therefore, the reduced significance of the intermolecular interactions (Hoy and Robbins, 2006).

Lastly, the yield strength reported in Fig. 13e shows a unique transitional behavior. For degradation under traction-free conditions, the yield strength decreases as the UV dose increases, which is a typical behavior expected due to chain scission (Wu and Buckley, 2004). However, for degradation at 16 MPa tensile, the yield strength is unaffected by photo-degradation. This can be attributed to the increased energy due to UV which allows for creep strain while under stress and leads to strain hardening. Therefore, the increase in free volume due to scission is balanced by strain hardening. Additionally, for degradation at 32 MPa, the yield strength increases as the UV dose

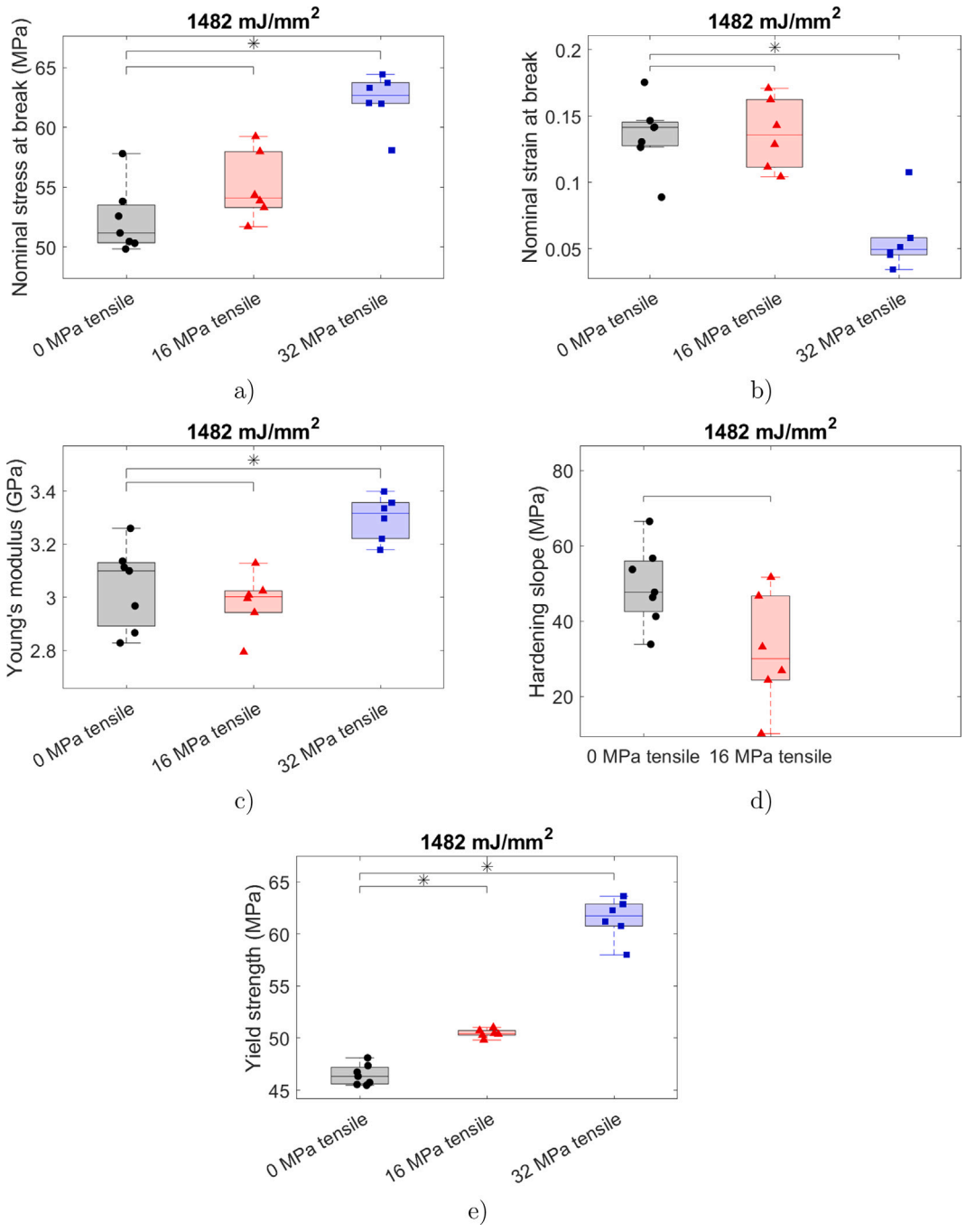

Fig. 16. Boxplots comparing the effect of applied stress on the (a) nominal stress at break, (b) nominal strain at break, (c) Young's modulus, (d) hardening slope, and (e) yield strength for a UV dose of 1482 mJ/mm^2. Note that an (∗) in the plots indicates statistical significance as a result of the Wilcoxon rank sum test (p-value < 0.05).

increases, suggesting that strain hardening is more dominant than the increase in free volume after a certain applied stress.

7. Conclusion

In this work, we have characterized the microscopic chemical changes and macroscopic constitutive changes due to photo-degradation with a focus on stress effects and the resulting mechanical behavior of cellulose acetate.

A comprehensive experimental program was conducted, consisting of first degrading cellulose acetate under traction-free conditions and under applied stress prior to testing the effect of degradation on the materials' response. The performed tests can be split into two groups: those that aim to uncover micro-scale chemical/molecular information and those that aim to uncover macro-scale mechanical behavior. Based on the results from the former set of experiments, it was observed that an increase in the UV dose decreases both M_w and T_g, without having any significant effect on the functional groups in cellulose acetate regardless of the applied stress. Based on the results from the latter set of experiments, it was observed that both the UV dose and applied stress affect the mechanical properties. These results suggest that upon photo-degradation, our material undergoes chain scission, which may be further affected by the applied stress. Moreover, the unique transitional behavior of the yield strength is due to a competition between scission and strain hardening under creep conditions.

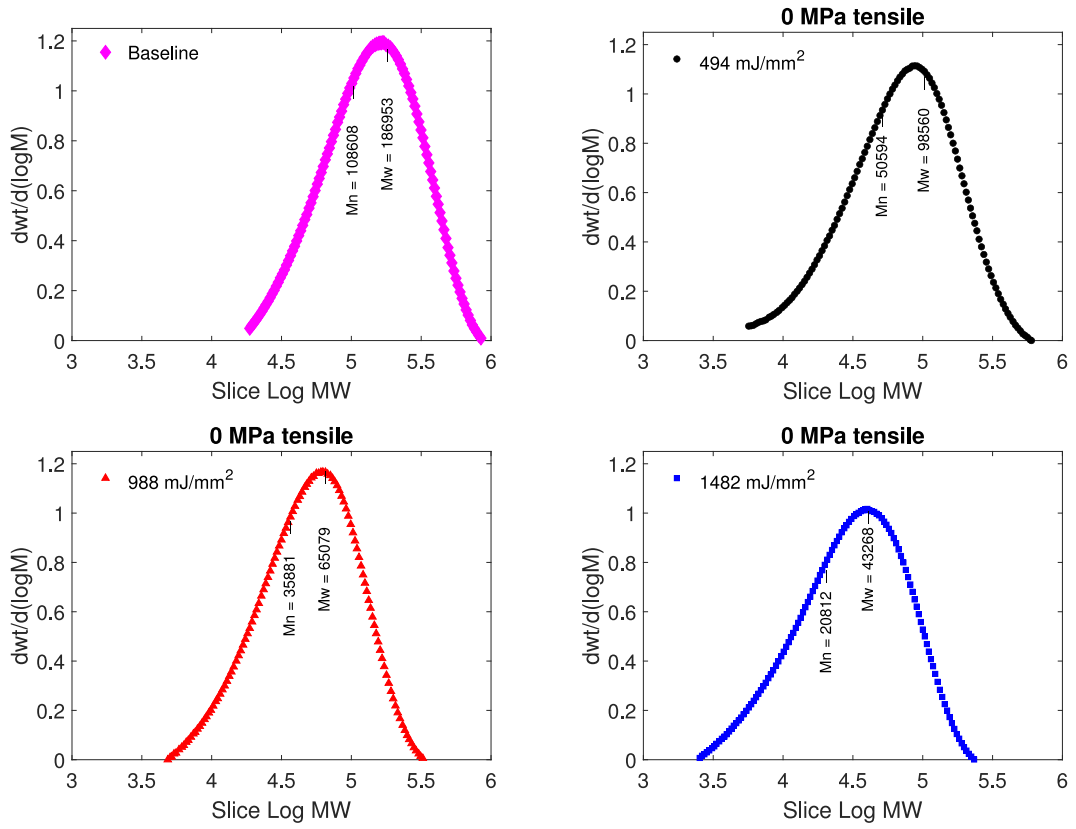

Fig. 17. GPC dwt/d(logM) — Slice log MW curves for cellulose acetate comparing the effect of the UV dosage under traction-free degradation.

The novelty of this work lies in its comprehensive approach that investigates the effect of photo-degradation on mechanical properties while simultaneously addressing stress effects and the underlying chemistry.

Our future research will focus on further experimental and modeling endeavors. Towards the experimental endeavors, it remains crucial to investigate rate-dependent phenomena such as strain rate-dependency and creep. Towards the modeling endeavors, we will develop constitutive models that incorporate stress-coupling that can be used for predicting photo-degradation for this class of materials, as it was shown that the applied stress has some significant effects on the constitutive behavior.

CRediT authorship contribution statement

Keven Alkhoury: Writing – original draft, Investigation, Conceptualization. **Chi Zhang:** Formal analysis. **Guangliang Liu:** Investigation. **Kathleen McEnnis:** Writing – review & editing. **Laurence Brassart:** Writing – review & editing. **Siva P.V. Nadimpalli:** Writing – review & editing, Supervision. **Shawn A. Chester:** Writing – review & editing, Supervision, Funding acquisition.

Declaration of competing interest

The authors declare that they have no known competing financial interests or personal relationships that could have appeared to influence the work reported in this paper.

Data availability

Data will be made available on request.

Acknowledgments

SAC acknowledges partial support from the National Science Foundation, USA under grant number (CMMI-1751520). SN acknowledges partial support from the National Science Foundation, USA under grant number (CMMI-2026717). The opinions, findings, and conclusions, or recommendations expressed are those of the author(s) and do not necessarily reflect the views of the National Science Foundation. LB acknowledges support from UK Research and Innovation under grant number [MR/W006995/1]. The authors gratefully acknowledge Prof. Frieder Jaekle and Mr. Xiao Luo from Rutgers University-Newark for their advice and for performing the GPC experiments. The authors are also grateful to Mr. Robert Ivko for his valuable assistance in the construction of the experimental setup.

Appendix A. Gel permeation chromatography (GPC) results

See Figs. 17–20.

Appendix B. Thermogravimetric analysis (TGA) results

See Figs. 21 and 22.

Appendix C. Differential scanning calorimetry (DSC) results

See Fig. 23.

Appendix D. Uniaxial tension test results

See Fig. 24.

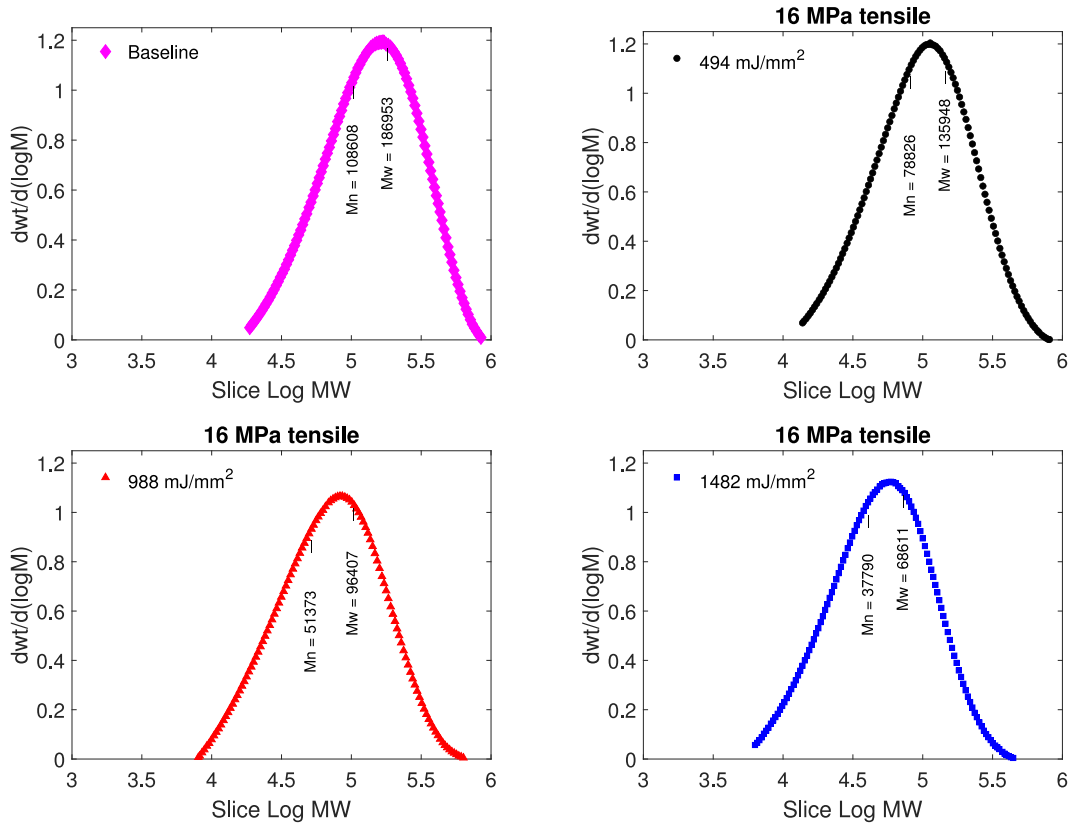

Fig. 18. GPC dwt/d(logM) — Slice log MW curves for cellulose acetate comparing the effect of the UV dosage on degradation under an applied stress of 16 MPa tensile.

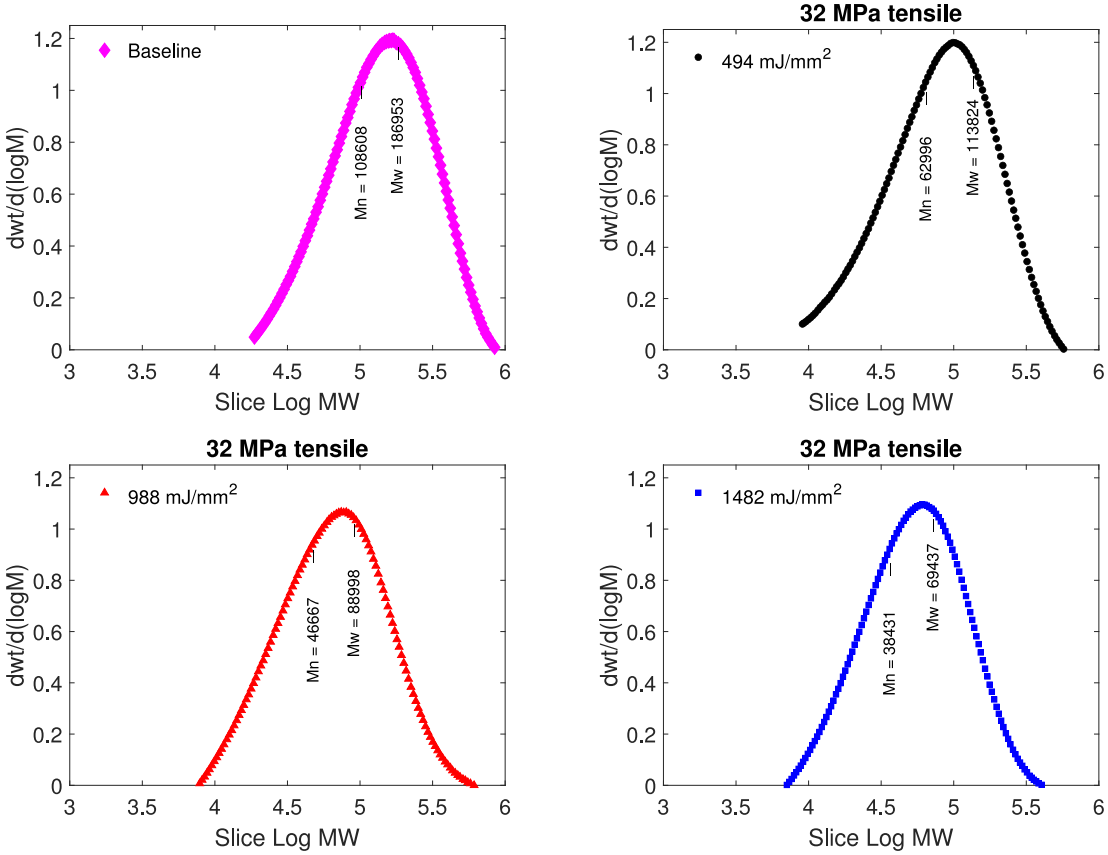

Fig. 19. GPC dwt/d(logM) — Slice log MW curves for cellulose acetate comparing the effect of the UV dosage on degradation under an applied stress of 32 MPa tensile.

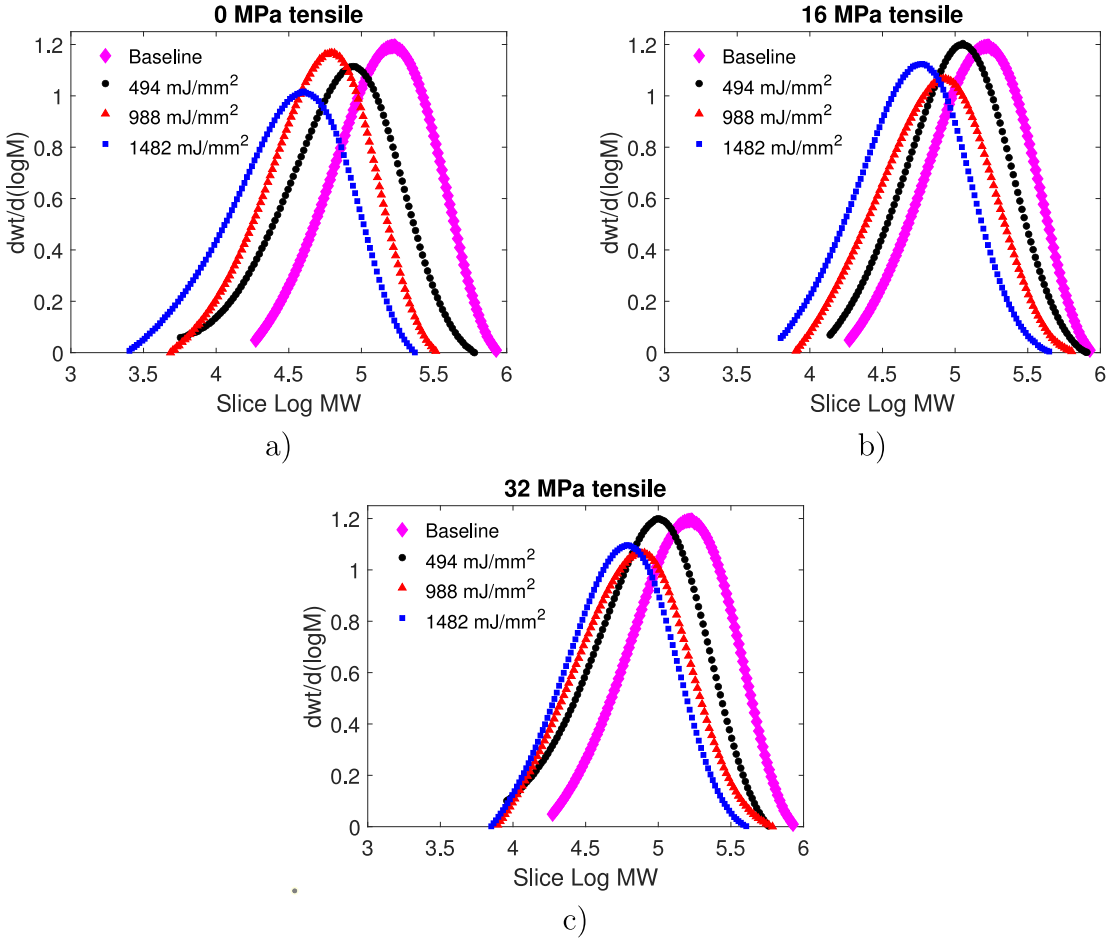

Fig. 20. GPC dwt/d(logM) — Slice log MW curves for cellulose acetate comparing the effect of the UV dosage on degradation under (a) traction-free conditions, (b) an applied stress of 16 MPa tensile, and (c) an applied stress of 32 MPa tensile.

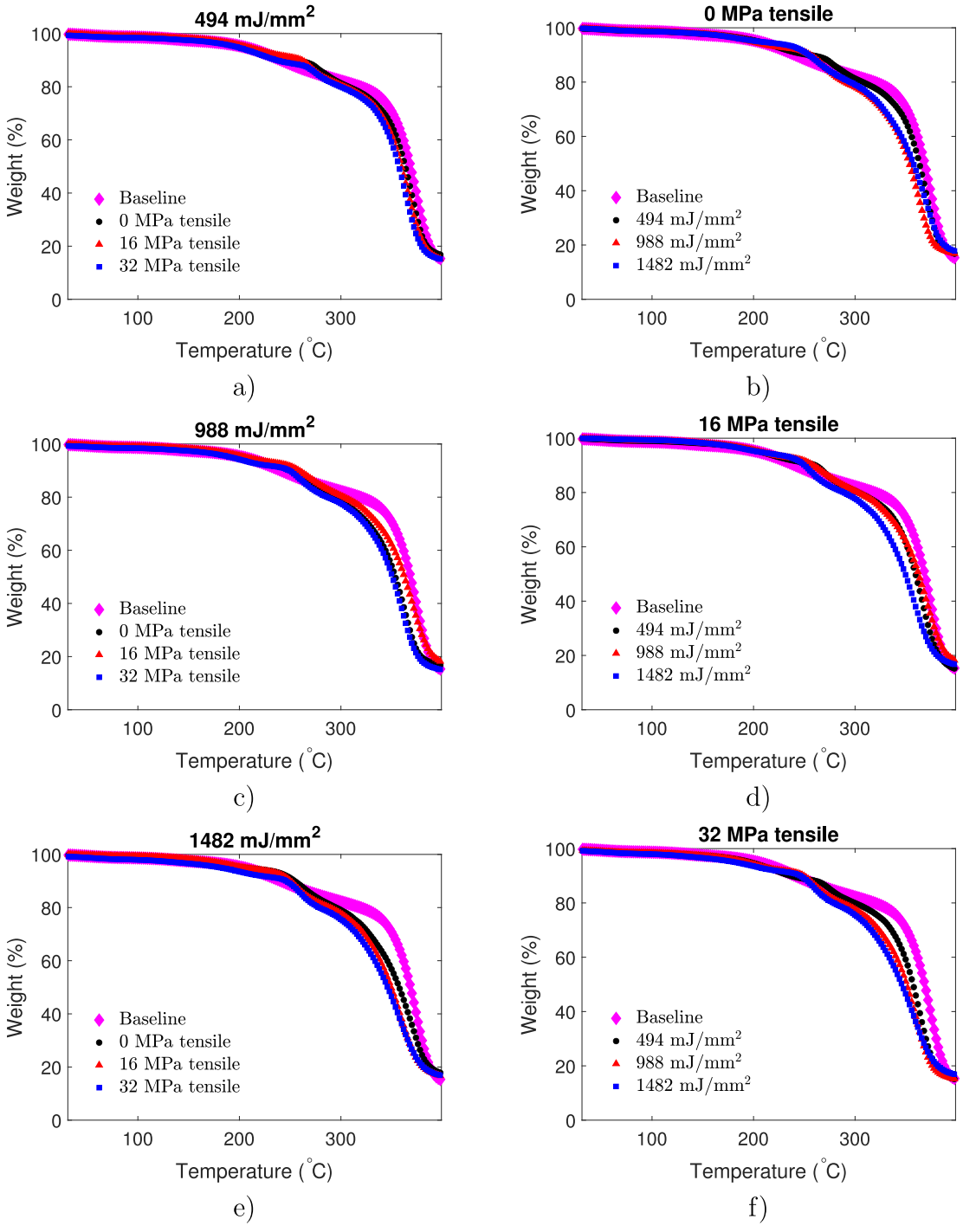

Fig. 21. TGA weight (%) — temperature (°C) results for cellulose acetate a, c, and (e) comparing the effect of the applied stress under the same UV dose, and b, d, and (f) comparing the effect of the UV dosage under the same applied stress.

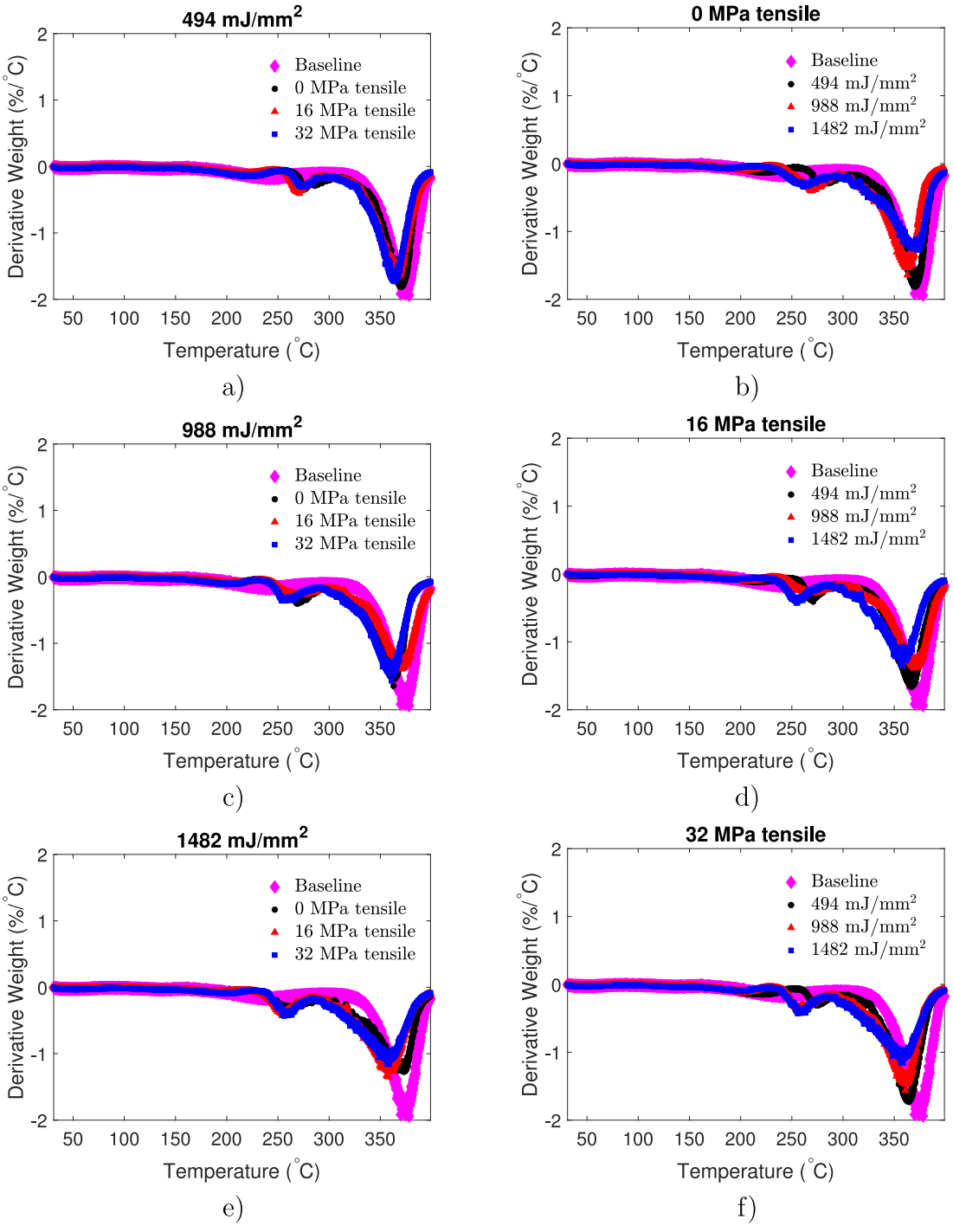

Fig. 22. TGA derivative weight (%/°C) — temperature (°C) results for cellulose acetate a, c, and (e) comparing the effect of the applied stress under the same UV dose, and b, d, and (f) comparing the effect of the UV dosage under the same applied stress.

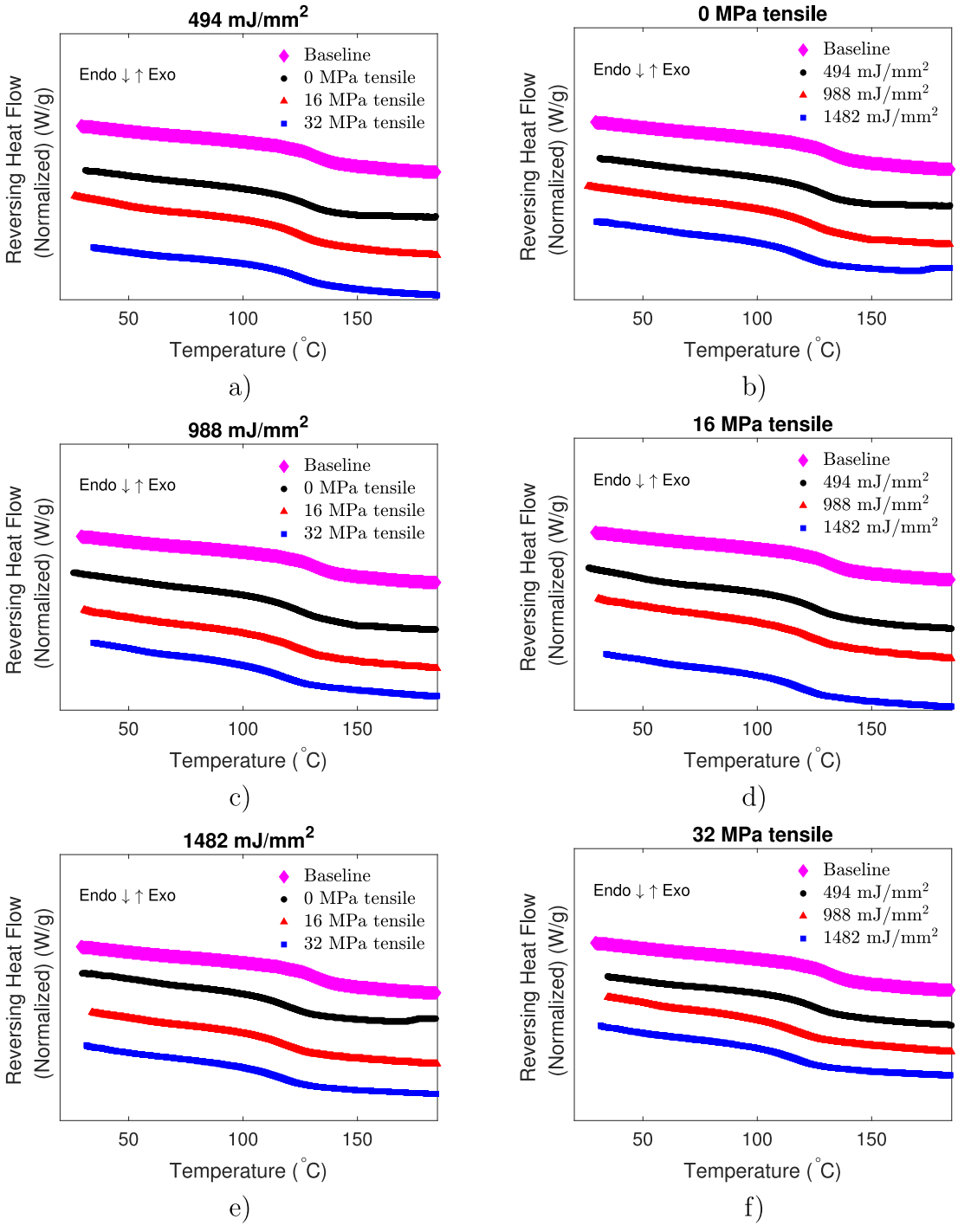

Fig. 23. DSC normalized reversing heat flow (W/g) — temperature (°C) curves for cellulose acetate a, c, and (e) comparing the effect of the applied stress under the same UV dose, and b, d, and (f) comparing the effect of the UV dosage under the same applied stress.

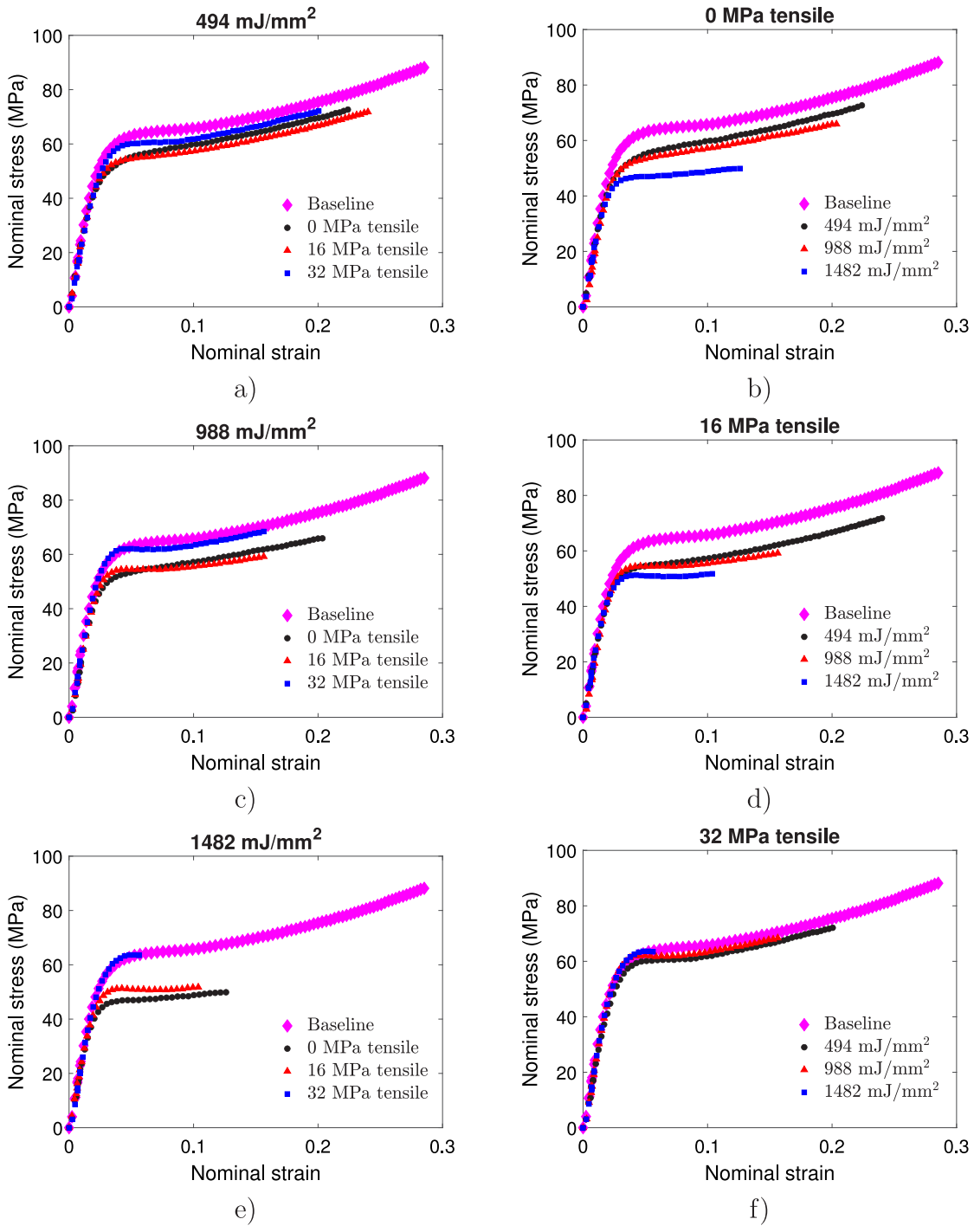

Fig. 24. Uniaxial experimental results for load–unload tensile tests for cellulose acetate a, c, and e) comparing the effect of the applied stress under the same UV dose, and b, d, and f) comparing the effect of the UV dosage under the same applied stress.

References

Al-Abri, M., Al-Ghafri, B., Bora, T., Dobretsov, S., Dutta, J., Castelletto, S., Rosa, L., Boretti, A., 2019. Chlorination disadvantages and alternative routes for biofouling control in reverse osmosis desalination. NPJ Clean Water 2 (1), 2.

Argon, A., Demkowicz, M., 2008. What can plasticity of amorphous silicon tell us about plasticity of metallic glasses? Metall. Mater. Trans. A 39, 1762–1778.

Asgher, M., Qamar, S.A., Bilal, M., Iqbal, H.M., 2020. Bio-based active food packaging materials: Sustainable alternative to conventional petrochemical-based packaging materials. Food Res. Int. 137, 109625.

Ayoub, G., Rodriguez, A., Mansoor, B., Colin, X., 2020. Modeling the visco-hyperelastic–viscoplastic behavior of photodegraded semi-crystalline low-density polyethylene films. Int. J. Solids Struct. 204, 187–198.

Barud, H.S., de Araújo Júnior, A.M., Santos, D.B., de Assunção, R.M., Meireles, C.S., Cerqueira, D.A., Rodrigues Filho, G., Ribeiro, C.A., Messaddeq, Y., Ribeiro, S.J., 2008. Thermal behavior of cellulose acetate produced from homogeneous acetylation of bacterial cellulose. Thermochim. Acta (ISSN: 0040-6031) 471 (1), 61–69. http://dx.doi.org/10.1016/j.tca.2008.02.009, URL https://www.sciencedirect.com/science/article/pii/S0040603108000506.

Belbachir, S., Zaïri, F., Ayoub, G., Maschke, U., Naït-Abdelaziz, M., Gloaguen, J.-M., Benguediab, M., Lefebvre, J.-M., 2010. Modelling of photodegradation effect on elastic–viscoplastic behaviour of amorphous polylactic acid films. J. Mech. Phys. Solids 58 (2), 241–255.

Briassoulis, D., 2005. The effects of tensile stress and the agrochemical vapam on the ageing of low density polyethylene (LDPE) agricultural films. Part I. Mechanical behaviour. Polym. Degrad. Stab. (ISSN: 0141-3910) 88 (3), 489–503. http://dx.doi.

org/10.1016/j.polymdegradstab.2004.11.021, URL https://www.sciencedirect.com/science/article/pii/S0141391005000029.

Celina, M.C., 2013. Review of polymer oxidation and its relationship with materials performance and lifetime prediction. Polym. Degrad. Stab. (ISSN: 0141-3910) 98 (12), 2419–2429. http://dx.doi.org/10.1016/j.polymdegradstab.2013.06.024, URL https://www.sciencedirect.com/science/article/pii/S014139101300195X.

Consolati, G., Nichetti, D., Quasso, F., 2023. Probing the free volume in polymers by means of positron annihilation lifetime spectroscopy. Polymers (ISSN: 2073-4360) 15 (14), http://dx.doi.org/10.3390/polym15143128, URL https://www.mdpi.com/2073-4360/15/14/3128.

Delplace, V., Nicolas, J., 2015. Degradable vinyl polymers for biomedical applications. Nat. Chem. 7 (10), 771–784.

Edgar, K.J., Buchanan, C.M., Debenham, J.S., Rundquist, P.A., Seiler, B.D., Shelton, M.C., Tindall, D., 2001. Advances in cellulose ester performance and application. Prog. Polym. Sci. (ISSN: 0079-6700) 26 (9), 1605–1688. http://dx.doi.org/10.1016/S0079-6700(01)00027-2, URL https://www.sciencedirect.com/science/article/pii/S0079670001000272.

Eerhart, A., Faaij, A., Patel, M., 2012. Replacing fossil based PET with biobased PEF; process analysis, energy and GHG balance. Energy Environ. Sci. 5 (4), 6407–6422.

Elsawy, M.A., Kim, K.-H., Park, J.-W., Deep, A., 2017. Hydrolytic degradation of polylactic acid (PLA) and its composites. Renew. Sustain. Energy Rev. (ISSN: 1364-0321) 79, 1346–1352. http://dx.doi.org/10.1016/j.rser.2017.05.143, URL https://www.sciencedirect.com/science/article/pii/S1364032117307876.

Fischer, S., Thümmler, K., Volkert, B., Hettrich, K., Schmidt, I., Fischer, K., 2008. Properties and applications of cellulose acetate. Macromol. Symp. 262 (1), 89–96. http://dx.doi.org/10.1002/masy.200850210, URL https://onlinelibrary.wiley.com/doi/abs/10.1002/masy.200850210.

Fox, Jr., T.G., Flory, P.J., 1950. Second-order transition temperatures and related properties of polystyrene. I. Influence of molecular weight. J. Appl. Phys. 21 (6), 581–591.

Galiano, F., Briceño, K., Marino, T., Molino, A., Christensen, K.V., Figoli, A., 2018. Advances in biopolymer-based membrane preparation and applications. J. Membr. Sci. (ISSN: 0376-7388) 564, 562–586. http://dx.doi.org/10.1016/j.memsci.2018.07.059, URL https://www.sciencedirect.com/science/article/pii/S0376738818313097.

Gardette, M., Perthue, A., Gardette, J.-L., Janecska, T., Földes, E., Pukánszky, B., Therias, S., 2013. Photo- and thermal-oxidation of polyethylene: Comparison of mechanisms and influence of unsaturation content. Polym. Degrad. Stab. (ISSN: 0141-3910) 98 (11), 2383–2390. http://dx.doi.org/10.1016/j.polymdegradstab.2013.07.017, URL https://www.sciencedirect.com/science/article/pii/S0141391013002395.

Hamid, S.H., 2000. Handbook of Polymer Degradation. CRC Press.

Hecht, E., 2002. Optics. Pearson Education Inc..

Hoy, R.S., Robbins, M.O., 2006. Strain hardening of polymer glasses: Effect of entanglement density, temperature, and rate. J. Polym. Sci. B 44 (24), 3487–3500.

La Mantia, F., Morreale, M., Botta, L., Mistretta, M., Ceraulo, M., Scaffaro, R., 2017. Degradation of polymer blends: A brief review. Polym. Degrad. Stab. (ISSN: 0141-3910) 145, 79–92. http://dx.doi.org/10.1016/j.polymdegradstab.2017.07.011, URL https://www.sciencedirect.com/science/article/pii/S014139101730201X Modification, Degradation and Stabilisation of Polymers: Concepts and Applications (MoDeSt 2016).

Lambert, J.H., 1760. Photometria Sive De Mensura Et Gradibus Luminis, Colorum Et Umbrae. sumptibus vidvae E. Klett, typis CP Detleffsen.

Mai, Y., Head, D., Cotterell, B., Roberts, B., 1980. Mechanical properties of nylon 6 subjected to photodegradation. J. Mater. Sci. 15 (12), 3057–3065.

Najmeddine, A., Xu, Z., Liu, G., Croft, Z.L., Liu, G., Esker, A.R., Shakiba, M., 2022. Physics and chemistry-based constitutive modeling of photo-oxidative aging in semi-crystalline polymers. Int. J. Solids Struct. 239, 111427.

Nakajima, H., Dijkstra, P., Loos, K., 2017. The recent developments in biobased polymers toward general and engineering applications: Polymers that are upgraded from biodegradable polymers, analogous to petroleum-derived polymers, and newly developed. Polymers 9 (10), 523.

Parida, S., Prabhu, S., Dinesh, T.K., Tyagi, K.K., 2022. A comprehensive study of biodegradation of cigarette filters and bidi butts. Contributions Tob. Nicotine Res. 31 (3), 151–161.

Pasparakis, G., Manouras, T., Argitis, P., Vamvakaki, M., 2012. Photodegradable polymers for biotechnological applications. Macromol. Rapid Commun. 33 (3), 183–198.

Rasselet, D., Ruellan, A., Guinault, A., Miquelard-Garnier, G., Sollogoub, C., Fayolle, B., 2014. Oxidative degradation of polylactide (PLA) and its effects on physical and mechanical properties. Eur. Polym. J. 50, 109–116.

Rodriguez, A., Mansoor, B., Ayoub, G., Colin, X., Benzerga, A., 2020. Effect of UV-aging on the mechanical and fracture behavior of low density polyethylene. Polym. Degrad. Stab. (ISSN: 0141-3910) 180, 109185. http://dx.doi.org/10.1016/j.polymdegradstab.2020.109185, URL https://www.sciencedirect.com/science/article/pii/S0141391020301178.

Santos-Sauceda, I., Castillo-Ortega, M., del Castillo-Castro, T., Armenta-Villegas, L., Ramírez-Bon, R., 2021. Electrospun cellulose acetate fibers for the photodecolorization of methylene blue solutions under natural sunlight. Polym. Bull. 78, 4419–4438.

Shyichuk, A., Stavychna, D., White, J., 2001. Effect of tensile stress on chain scission and crosslinking during photo-oxidation of polypropylene. Polym. Degrad. Stab. (ISSN: 0141-3910) 72 (2), 279–285. http://dx.doi.org/10.1016/S0141-3910(01)00015-5, URL https://www.sciencedirect.com/science/article/pii/S0141391001000155.

Tsuji, H., Echizen, Y., Nishimura, Y., 2006. Photodegradation of biodegradable polyesters: A comprehensive study on poly (l-lactide) and poly (ϵ-caprolactone). Polym. Degrad. Stab. 91 (5), 1128–1137.

Van de Velde, K., Kiekens, P., 2002. Biopolymers: overview of several properties and consequences on their applications. Polym. Test. (ISSN: 0142-9418) 21 (4), 433–442. http://dx.doi.org/10.1016/S0142-9418(01)00107-6, URL https://www.sciencedirect.com/science/article/pii/S0142941801001076.

White, J., Shyichuk, A., 2007. Macromolecular scission and crosslinking rate changes during polyolefin photo-oxidation. Polym. Degrad. Stab. (ISSN: 0141-3910) 92 (7), 1161–1168. http://dx.doi.org/10.1016/j.polymdegradstab.2007.04.011, URL https://www.sciencedirect.com/science/article/pii/S0141391007001437.

Wu, J., Buckley, C., 2004. Plastic deformation of glassy polystyrene: A unified model of yield and the role of chain length. J. Polym. Sci. B 42 (11), 2027–2040.

Yadav, N., Hakkarainen, M., 2021. Degradable or not? Cellulose acetate as a model for complicated interplay between structure, environment and degradation. Chemosphere (ISSN: 0045-6535) 265, 128731. http://dx.doi.org/10.1016/j.chemosphere.2020.128731, URL https://www.sciencedirect.com/science/article/pii/S0045653520329295.

Yousif, E., Haddad, R., 2013. Photodegradation and Photostabilization of Polymers, Especially Polystyrene. vol. 2, SpringerPlus, pp. 1–32, (1).

Zhu, Y., Romain, C., Williams, C.K., 2016. Sustainable polymers from renewable resources. Nature 540 (7633), 354–362.